

THESIS ON MECHANICAL ENGINEERING E106

Investigation of Severe Plastic Deformation Processes for Aluminum Based Composites

AGUS PRAMONO

TUT
PRESS

TALLINN UNIVERSITY OF TECHNOLOGY
Faculty of Mechanical Engineering
Department of Materials Engineering

Dissertation was accepted for the defense of degree of Doctor of Philosophy in Engineering on November 15, 2016.

Supervisor: Lauri Kollo, Ph.D.
Department of Materials Engineering, Tallinn University of Technology

Co-Supervisor: Lembit Kommel, Ph.D.
Department of Materials Engineering, Tallinn University of Technology

Opponents: Professor Michal Besterci, Institute of Materials Research,
Slovak Academy of Sciences, Slovak Republic

Tõnu Roosaar, Ph.D. Inspecta Estonia OÜ.

Defense of the thesis: December 19, 2016

Declaration:

Hereby I declare that this doctoral thesis, my original investigation and achievement, submitted for the doctoral degree at Tallinn University of Technology, has not been submitted for any academic degree.

/Agus Pramono/



Copyright: Agus Pramono, 2016
ISSN 1406-4758
ISBN 978-9949-83-044-2 (publication)
ISBN 978-9949-83-045-9 (PDF)

MEHHAOTEHNIKA E106

Alumiiniumi baasil komposiitide süvoplastse deformatsiooni protsesside uurimine

AGUS PRAMONO

CONTENTS

FOREWORD	7
ABBREVIATIONS AND SYMBOLS	8
INTRODUCTION	10
1 LITERATURE REVIEW	11
1.1 General overview	11
1.2 Overview of the severe plastic deformation methods	13
1.3 Equal channel angular pressing (ECAP)	13
1.4 Equal parallel channel angular pressing (ECAP-PC)	18
1.5 Accumulative roll bonding (ARB)	22
1.6 Latest development in SPD	27
1.7 Heat treatment of aluminum alloys	29
1.8 Main objectives of the thesis	32
2 EXPERIMENTAL PROCEDURES AND MATERIALS	34
2.1 Materials	34
2.1.1 Materials for ECAP and ECAP-PC	34
2.1.2 Materials for ARB and RPRB	34
2.2 Ball milling process of aluminum powder based composite	34
2.3 ECAP methods and processes	35
2.4 Heat treatment	36
2.5 Accumulative roll bonding process	37
2.6 Repetitive press roll bonding process	38
2.7 Study of microstructure and properties	38
3 RESULT AND DISCUSSION	39
3.1 Aluminum alloys by ECAP consolidation	39
3.1.1 Microstructure and properties of ECAP consolidated alloys	39
3.1.2 Mechanical properties of ECAP consolidated alloys	42
3.2 Aluminum based composite by ECAP-PC consolidation	45
3.2.1 Microstructure	45
3.2.2 Mechanical properties	46
3.3 Aluminum based composite by ARB	50
3.3.1 Microstructure	50
3.3.2 Mechanical properties	53
3.3.3 Determination of the parameters of the ARB process using the FEM analysis	55
3.3.4 Microstructure evolution of Al based composite after the second cycle of ARB	60
3.4 Aluminum based composites by RPRB	61
3.4.1 Microstructure	61
3.4.2 Mechanical properties	61
3.4.3 Evolution of microstructure in the RPRB process	64
CONCLUSIONS	65

REFERENCES	67
LIST OF PUBLICATIONS	74
ACKNOWLEDGEMENTS	75
ABSTRACT	76
KOKKUVÕTE	77
ELULOOKIRJELDUS	78
CURRICULUM VITAE	80

FOREWORD

Metal forming by Severe Plastic Deformation (SPD) evolves rapidly among the manufacturing technologies. The main emerging technologies next to forging and extrusion are Equal Channel Angular Pressing (ECAP) and Accumulative Roll Bonding (ARB).

Development of metal alloys is a well-advanced research area research interests in metal matrix composites (MMCs) are increasing. MMCs have been produced by several processes: casting, powder metallurgy and metal forming processes. One of the potential compaction routes involving effective mixing of reinforcement particulates with grain refinement is SPD. Initially, SPD was developed for aluminum alloys. Today some processes are applicable also for MMCs. There are three basic process of SPD: ECAP, High Pressure Torsion (HPT) and ARB.

Variations in SPD technologies developed have improved the effectiveness of grain refinement, ability to process materials of higher strength or remaining the sample integrity during the process. The main methods are ECAP with Parallel Channels, Continuous-HPT and Repetitive Press Roll Bonding (RPRB).

Consolidation of powder materials by SPD is capable of generating increased properties compared to standard SPD, as grain refinement is accompanied with particle reinforcement. Some of SPD processes like ECAP and ARB have been developed for industrial applications.

Heat treatment is often an essential step used with the SPD process to manipulate the properties of materials, one of which is to improve formability. To improve the mechanical properties by heat treatment using solid solution treatment (T6) normally is applied to obtain higher mechanical properties. Nevertheless, still a large number of passes of ECAP and cycles of ARB are required. To decrease the need for high number of repetitions, a novel SPD process, such as RPRB, combined of pressing and rolling, has evolved. Pressing process before rolling will provide higher bonding at the interphase between the matrix and the reinforcement to produce increased properties in fewer cycles.

The current research is focused on the use of SPD technology for composite materials. Superior mechanical properties can be expected when combining metal materials, such as aluminum with ceramic materials, for instance Al_2O_3 nanofiber. Modern transportation industry is continuously looking for materials with higher specific strength and stiffness.

ABBREVIATIONS AND SYMBOLS

AA1070	- Aluminum alloys series 1070
AA6061	- Aluminum alloys series 6061
AA7075	- Aluminum alloys series 7075
ACE	- Accumulative Continuous Extrusion
As-ECAP	- Samples without heat treatment
AlPoCo	- Aluminum Powder Company Ltd
ANF	- Al ₂ O ₃ nanofibers
APB	- Accumulative Press Bonding
ARB	- Accumulative Roll Bonding
C-HPT	- Continuous High Pressure Torsion
CP	- Cold Pressing
CR	- Cold Regions
ECAE	- Equal Channel Angular Extrusion
ECAP	- Equal Channel Angular Pressing
ECAP-C	- Equal Channel Angular Consolidation
ECAP-PC	- Equal Parallel Channel Angular Pressing
ECAP-BP	- Back Pressure Equal Channel Angular Pressing
ECAR	- Equal Channel Angular Rolling
ECAT	- Equal Channel Angular Torsion
FEM	- Finite Element Methods
GP	- Guinier Preston
HP	- Hot Pressing
HPT	- High Pressure Torsion
HR	- Hot Regions
MMC	- Metal Matrix Composites
MRAE	- Multi Rolling Angular Extrusion
NP	- Neutral Plane
O	- Annealing
RPRB	- Repetitive Press Roll Bonding
RPM	- Rotation per Minute
RSS	- Reversed Shear Spinning
SEM	- Scanning Electron Microscope
SPD	- Severe Plastic Deformation
T6	- Solid Solution Treatment
UFG	- Ultrafine Grained
XRD	- X ray Diffraction

- σ_y - yield strength
- σ_o - friction stress
- k_y - constant of yielding
- d - grains size
- d_c - diameter of ECAP sample
- ε - plastic strain
- ε_{eq} - magnitude of effective strain (For ECAP)
- equivalent strain (For ARB)
- γ - pressure shear
- k - the channel displacement
- N - number of passes
- n - number of cycles
- t_r - the rolling time (steady)

$d\varepsilon_{eq}/dt$ -the incremental equivalent strain

$-d\varepsilon_{yy}/dt$ -the plane strain condition, equivalent strain

$d\gamma_{xy}/dt$ -the incremental shear strain

- τ_f - the shear stress
- γ - the total shear strain
- \emptyset - angle of die
- r_t - total reduction
- t - thickness
- t_0 - initial thickness on the strips
- $wt\%$ - weight fraction
- ε - strain
- φ - the angle of intersection

INTRODUCTION

MMCs as a group of advanced materials that can lead to superior properties such as light weight, high strength, low thermal expansion coefficient and high wear resistance. The main reasons for using aluminum as the matrix are its high malleability, ductility and formability. Several series of aluminum alloys (AA) that have different properties for various applications have been developed [1-3].

Technologies of SPD, such as ECAP, HPT and ARB, have been used increasingly also for the development of composite materials. Primary compaction of composite powders can be done by ECAP by simple mixing of reinforcement particles with matrix powders, applying these in cans and passing the cans through an ECAP die. Ultrafine Grained (UFG) materials can be produced at full densification. Therefore, grain miniaturization can be coupled by reinforcement from particulates for mechanical property enhancement [4-7].

Standard ECAP dies produce billets through single abrupt angle with remaining defects and distortions in both ends of the billet. In practice, this thrives to loss of material and therefore to increased processing cost. An alternative procedure has been developed in which ECAP uses two parallel channels. During the process of parallel channels (ECAP-PC), two distinct shearing events take place during a single pass. During the processes on ECAP-PC there is a considerable reduction in the number of passes that is required for the formation of an ultrafine-grained structure at reduced wastage of material [8-9].

ARB is a roll-bonding process that causes accumulatively intense plastic straining. This results in ultra-fine grains and simultaneous inclusion of oxides from the surface uniformly to disperse into a material [10]. ARB processes are suitable for mass production also for aluminum composite materials, requiring up to 8-10 cycles in order to receive UFG material. It will produce uniform microstructures that increase mechanical properties. In this work, the author has made attempts to use the novel process named RPRB, combining ARB with uniaxial pressing to reduce the number of cycles to achieve an ultrafine structure.

1. LITERATURE REVIEW

1.1 General overview

Manufacturing technology of metal alloys and aluminum matrix composites is evolving from conventional technology to high pressure deformation. MMC with discontinuous shaped or fiber reinforcements offers discrete rigid ceramic reinforcements embedded in ductile metal alloys. Commonly, the addition of fibers as reinforcement increases the hardness and decreases the relative density [11-12].

SPD is a processing technique for alloys and composites with decreased grain size for varying polycrystalline samples [13-15]. A number of SPD technologies have been developed, ECAP and ARB being most well-known. Both of them are applied industrially in different fields, as seen in Fig 1.1 [15]. Markets for nanostructured materials by the SPD process exist in the sectors where superior properties, like specific strength or increased fatigue life, are needed. Formal market analysis specializing in nanostructured metals, conducted by company Metallicum, has found more than 100 specific markets for nanometals in aerospace, transportation, medical equipment, chemical processing, electronics and defense [16]. Some of the applications that use SPD materials are aluminum based composites with high yield strength and superplastic properties, higher mechanical properties in cold and cryogenic temperatures and high-strength lightweight TiNi alloys with shape-memory effect for space, medical and many other applications [15-16].

The development of ECAP has revealed some improved methodologies, such as Back Pressure-ECAP and Parallel Channel-ECAP developed recently [17-18]. The result of the development of ARB is the cross rolling to obtain more effective compression during cycles. Also, the addition of pressing before the rolling process to obtain a good bonding interface has been introduced. The SPD method enables basically production of a material with UFG size below $1\mu\text{m}$ to improve the mechanical properties. Different techniques and placement of SPD to illustrate the different grain sizes resulting for each method are shown in Fig 1.2 [19].

Methods of SPD, such as ECAP and ARB and several other methods have been designed specifically for certain applications with different characteristics [20]. They are very diverse in deformation mode, which can range from pure shear to simple shear as well as from monotonic to cyclic loads and cross loading. UFG with a fine grain size will result in the higher properties [20-21]. SPD technologies are usually applicable for mass production with variations of size of the billets. Only HPT is limited to a small size [15-16].

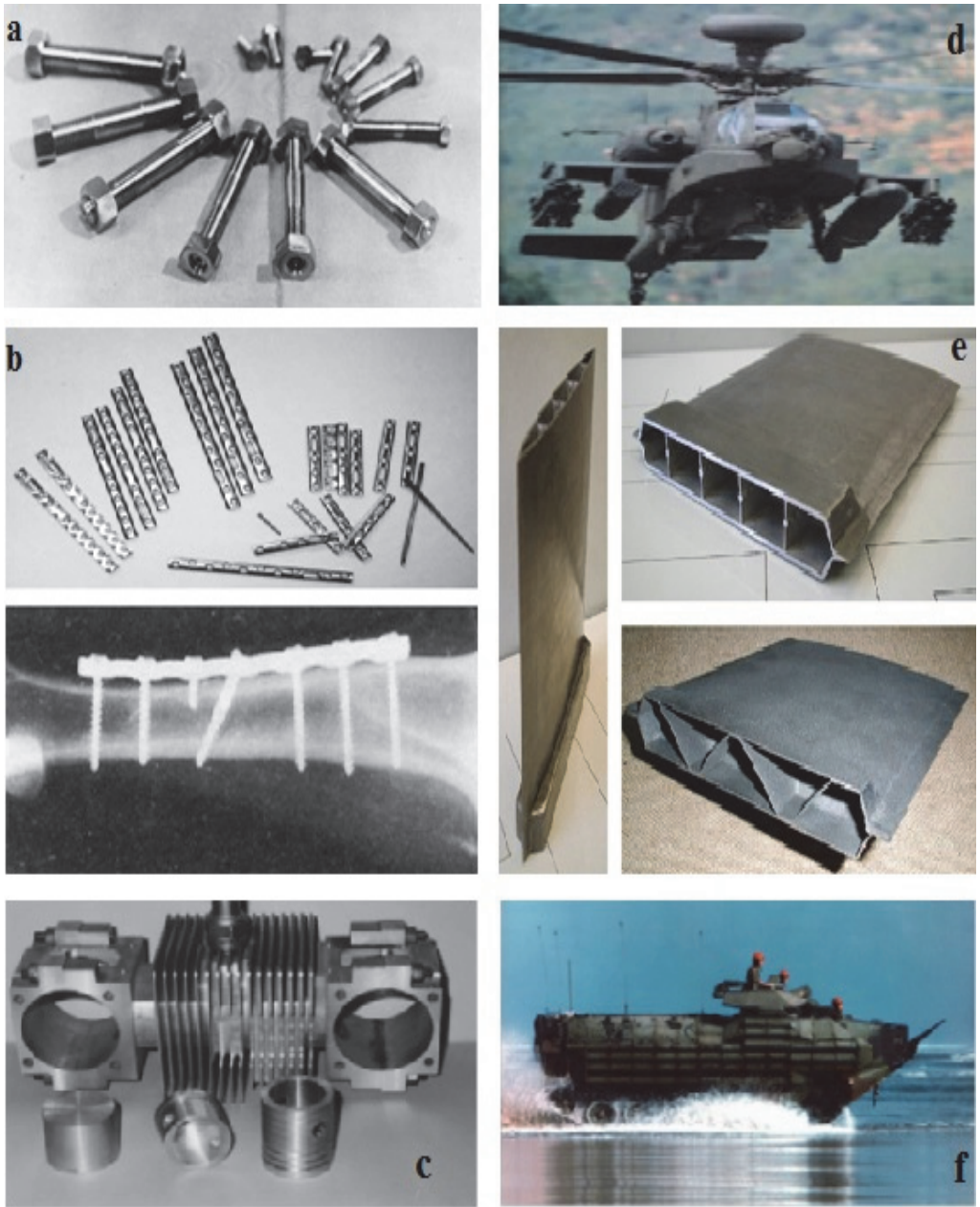


Figure 1.1 Application areas of ECAP and ARB: a) high strength thread out of SPD; b) plate implants made of SPD nanostructure; c) engine block machine fabricated from nanostructured AA1420; d) body of military helicopter from high strength materials; e) UFG Ti-6Al-4V super-plasticity sheet materials for Models of hollow blades f) military device - amphibious assault vehicle, courtesy of BAE Systems [15-16].

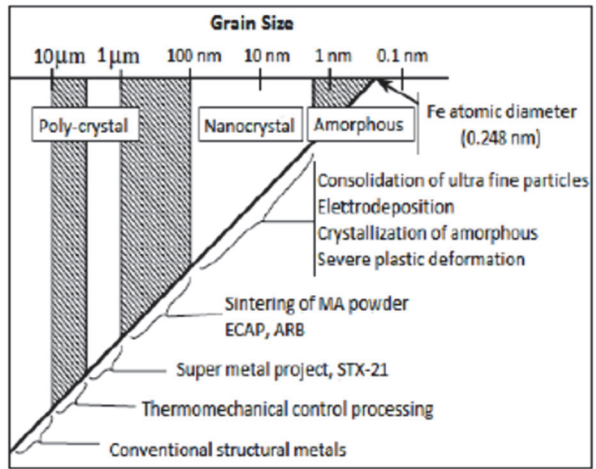


Figure 1.2 Manufacturing methods of UFG materials regarding obtainable grain size range [19].

1.2 Overview of the severe plastic deformation methods

Severe plastic deformation (SPD) is the process of forming considerable plastic strain by applying high pressure to obtain bulk UFG materials [22-23].

Type of SPD	Schematic Illustrations	Plastic Strain values
Equal Channel Angular Pressing (ECAP)		$\varepsilon = n \frac{2}{\sqrt{3}} \cot(\omega)$
High Pressure Torsion (HPT)		$\varepsilon = \frac{\gamma(r)}{\sqrt{3}}, \gamma(r) = n \frac{2\pi r}{t}$
Accumulative Roll Bonding (ARB)		$\varepsilon = n \frac{2}{\sqrt{3}} \ln\left(\frac{t_0}{t}\right)$

Figure 1.3 Three types of the first SPD technologies developed.

SPD is able to produce high strength lightweight materials with superplastic properties. SPD can introduce plastic strains higher than conventional processes, like forging, rolling, extrusion and drawing [15]. Three primary types of SPD technologies are ECAP, ARB and HPT, presented in Fig 1.3 with schematic illustration and the plastic strain values. There are a number of basic processing parameters important for the improvement of microstructure. Consideration is directed to features that significantly derive from the microstructure produced by the SPD technique in single crystalline, polycrystalline and MMCs [24-25].

1.3 Equal channel angular pressing (ECAP)

ECAP is a pressing process where compression and tensile forces are applied in angular die. The grain size of the resulting material achieves sub-micrometer size, which could produce unusual properties [24]. Application of pressure in ECAP processes shear stress as well as the pure and simple shear of monotonic load to cyclic loading and cross in the mold [17-19]. An advantage of ECAP compared to conventional metal working processes, like forging or extrusion, is the ability to achieve a high strain without dimensional changes of samples [26].

Principles of ECAP processing

Processing regimes of ECAP have been determined for most of metal alloys, but studies for compaction of MMC powders are still rare. Samples for ECAP are commonly in the form of bars or rods, the process can be applied also to plate samples. Figure 1.4 shows a schematic model of the ECAP procedure. ECAP die has a channel that is bent under corner, most commonly through 90° , as in Fig 1.5. The rod moves through the dies. The dimensions of the sample before and after pressing are unchanged and therefore allow unlimited number of passes to further refine the grains [23, 26-27].

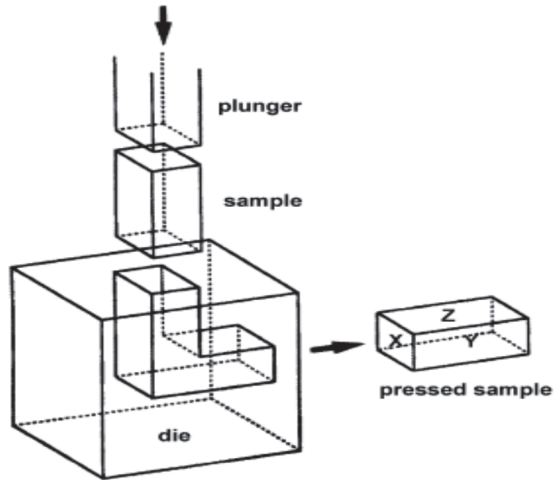


Figure 1.4 Schematic models of a typical ECAP dies facility: the X, Y and Z planes to determine the best direction transverse or longitudinal to determine changes in the microstructure [27].

The force exerted when deformation working is a simple shear as operational pressure, shear stress field can be illustrated by the trajectory; x, y and z, as in Fig. 1.4. Angle of the die is 90° , in the field of sliding in Fig 1.5, visible changes shown are in the number 1 to 2, which theoretically indicates a shift of material atoms that can improve mechanical properties [28].

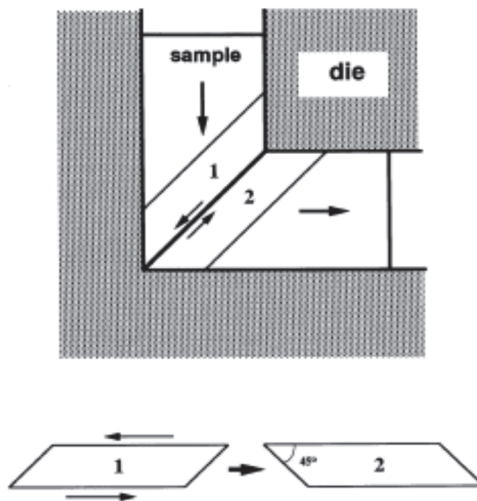


Figure 1.5 The principle of ECAP that explains the shearing plane on the ECAP die: 1) the change in direction of the force of the compression pressure; 2) with a shift angle 45° toward tensile stress [24].

To produce variable mechanical properties and grain distribution, different ECAP routes are used. The route of ECAP processing is distinguished by turning the samples under predefined angle between the passes, usually 90° and 180° , depending on the microstructures desired by ECAP [24]. The four regimes of ECAP processing routes are shown in Fig. 1.6. Route A is free from the rotation. During the route B_A , the sample is turned alternately with the reverse direction and under the angle of 90° . In route B_C , the rotation on the routes samples is conducted without reversing the direction of pressing, by consecutive passes under 90° between each pass. In route C, the sample is rotated by 180° between the passes. Combinations of these routes are allowed as well, for example, combining B_C and C of routes by alternating rotations through 90° and 180° after a couple of passes in the regime of ECAP [23-24].

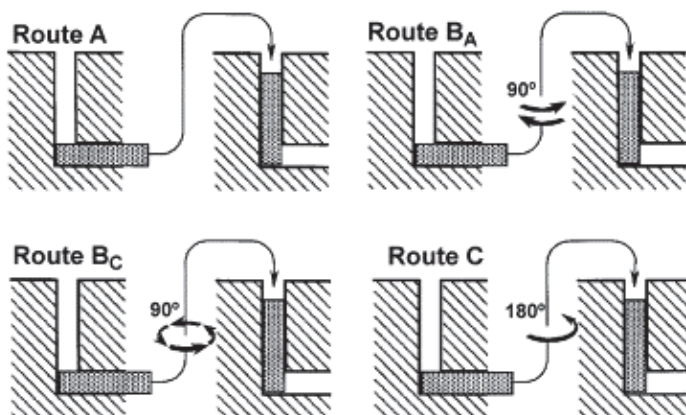


Figure 1.6 Four fundamental ECAP processing routes [24].

ECAP Consolidation

ECAP Technology is generally applied to solid objects such as in the form of bars or cylinders, but ECAP can be applied also for consolidation of powder. Important differences of pressing of powders are cracks that evolve more easily on the surface. In order to avoid cracking during consolidation, powder is put in a tight outer jacket, as shown in Fig 1.7. Results of previous research [23] have produced flawless materials, normally by use of heating during pressing. This means that compaction of alloy powders is possible by wrapping the powder and heating the die [4, 24].

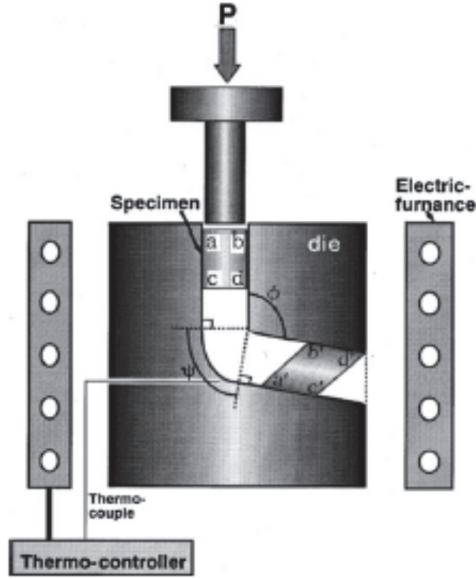


Figure 1.7 The ECAP consolidations of powder materials of powder: powder sample is wrapped to avoid defects when pressed [24].

Evolution microstructure during ECAP

Pressing by ECAP introduces simple shear on the material through the dies of channel maximizing the strain [23]. The strain magnitude obtained with 1 pass is a main advantage of this method. Shear stress occurs in the same plane during the process of continuously passed ECAP regimes, after reaching the intersection angle of ECAP die, so sliding direction turned around as assembled in Fig. 1.5 after a uniform strain distribution, the amount of shear (γ) can be calculated by assuming friction condition [28-29].

$$\gamma = 2 \cot\left(\frac{(\phi + \psi)}{2}\right) + \psi \operatorname{cosec}\left(\frac{(\phi + \psi)}{2}\right) \quad (1.1)$$

Effective strain (ϵ) is calculated, which is the result of ECAP after N passed, given by the following relationship:

$$\epsilon_{eq} = \frac{N}{3^{1/2}} \left[2 \cot\left(\frac{(\phi + \psi)}{2}\right) + \psi \cosh\left(\frac{(\phi + \psi)}{2}\right) \right] \quad (1.2)$$

Equation (1.2) describes effective strain on the ECAP sample during the whole process.

Internal pressure of ECAP in the die walls able to promote on the slip plane, after the pressure reaches the bend angle, the materials are strained. In this condition,

dislocation builds up and grain size is eventually reduced. This refinement mechanism is dislocation in the form of twinning (Fig. 1.8). Twinning mechanism works at low temperatures, with a temperature decrease, so the slip atomic zone increases sharply. This makes the grain to be finer, up to UFG with a required number of passes [30-31].

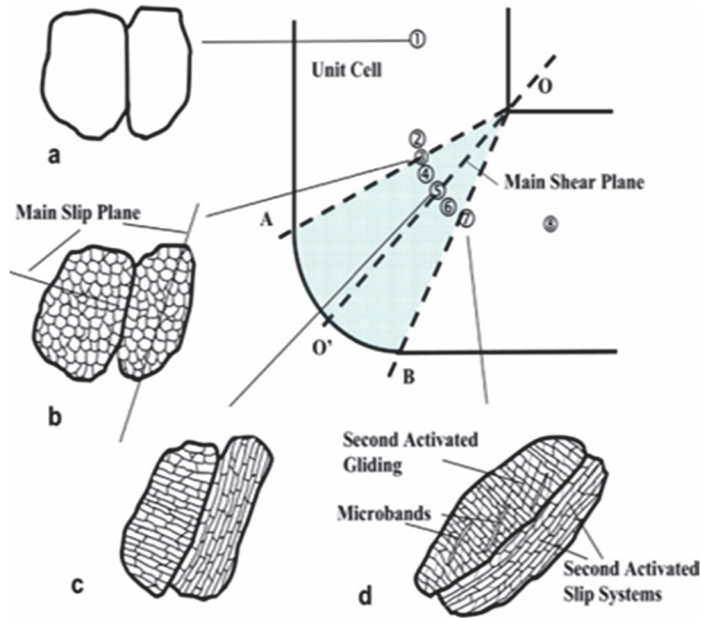


Figure 1.8 Schematic representation of microstructure evolution passed of the ECAP process: (a) the coarse grains before going through angle; (b) the movement of dislocations due to the narrowing of pressure; (c) gliding slip planes resulting in dislocation walls turned into motion twinning; (d) movement of secondary slip and micro bands [31].

1.4 Equal parallel channel angular pressing (ECAP-PC)

Consolidation during ECAP has evolved to using a facility which contains two parallel channels, namely ECAP-PC. A schematic model of die ECAP-PC is shown in Fig. 1.9, where φ is the intersection of parallel channels and K is the displacement of the channel. During ECAP-PC, two major events take place, for the movement of grains between the two channels there is a significant reduction in the number of passes that can produce UFG materials. The values for the displacement between the two channels, K, and the angle of intersection of the channels, φ , are the main parameters of the die geometry that must be considered [30].

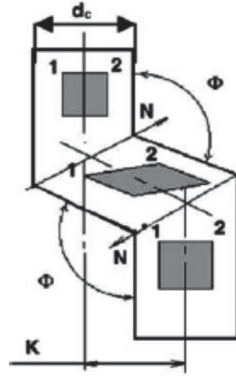


Figure 1.9 Schematic illustrations of ECAP-PC. N is the shear of direction, K constitutes displacement of two channels, ϕ represents the angle of intersection among two parts by the internal channel, shaded areas showing the shearing of the sample traverses on the shearing zone [30].

ECAP-PC process was developed to reduce the restrictions of conventional ECAP. It has been established that the optimal values of processing parameters, leading to the largest strain homogeneity in the cross-section of the pressed billet, are $\phi = 100^\circ$ and a displacement value of $K \approx d_c$, where d_c is the diameter of the channel. This could mean that the condition is achieved when the displacement between the two channels, the accumulated strain of the pass equals 2 times of the conventional ECAP [30-34]. Pressing process of ECAP-PC is shown in Fig. 1.10.

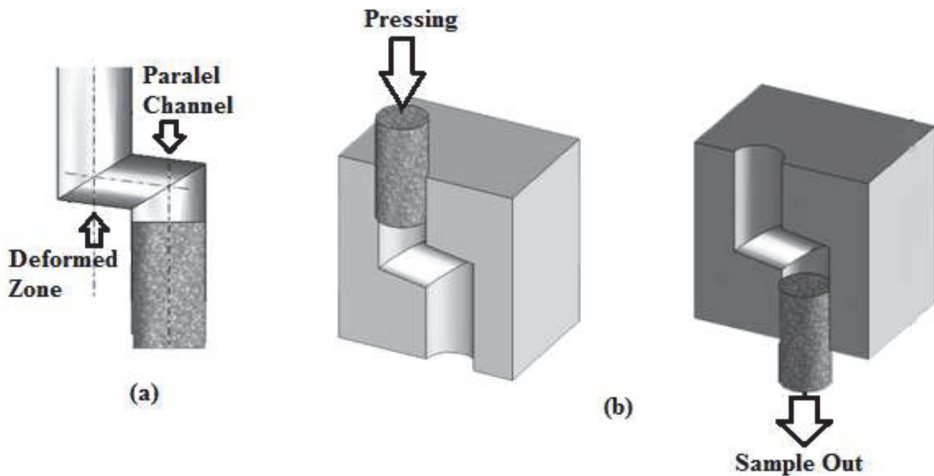


Figure 1.10 Representative scheme of ECAP-PC: (a) Pressing process on the deformation zone; (b) sample after pressing.

Effect of pressing during ECAP-PC

Based on the FEM investigation, the angle affects strongly the success of the ECAP-PC [35]. With the variation in the die channel angle and channel displacement the effective strain can be plotted under different conditions of displacement as seen in Fig. 1.11. Uniform pressure is generated from the angle of 120° , resulting from the effect of friction which is small, in some cases, when the pressing reaches the die angle, there will be a reduction in the channel length, and as a result, it will provide an effective strain. Decreasing the channel angle from 120° to 75° reduces the strain from 2.36 to 1.27. At lower effective strain 120° , $l=2d$ and the highest effective strain is correlated to 75° , $l=d$. However, this angle resulted in defects at some point when the sample was processed in cold conditions [35-37].

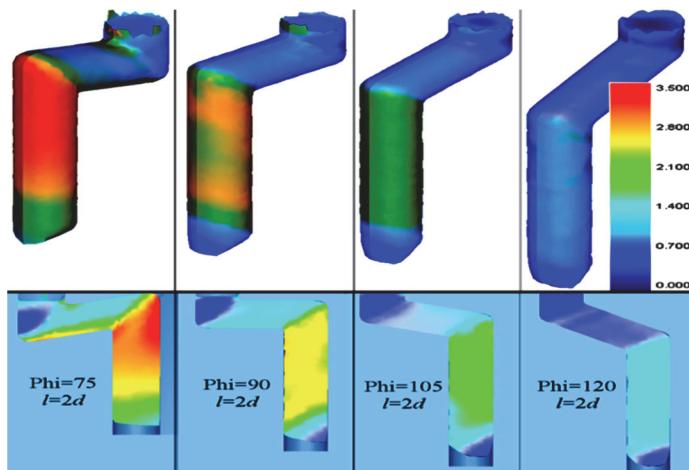


Figure 1.11 Difference of channel cross-section of a parallel channel to the process of pressing effect, respectively - each corner produces characteristic differences of properties [35].

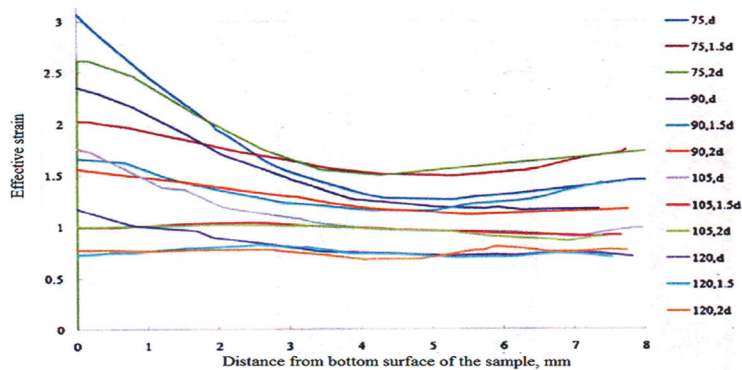


Figure 1.12 Influence sections of displacement channels on the effective strain at one pass on ECAP-PC, adapted from [36].

The relationship between the angles of channels against the effective strains for the channel displacement of $\geq 1.5d$ produces uniform strain, irrespective of the die angle, as shown in Fig. 1.12.

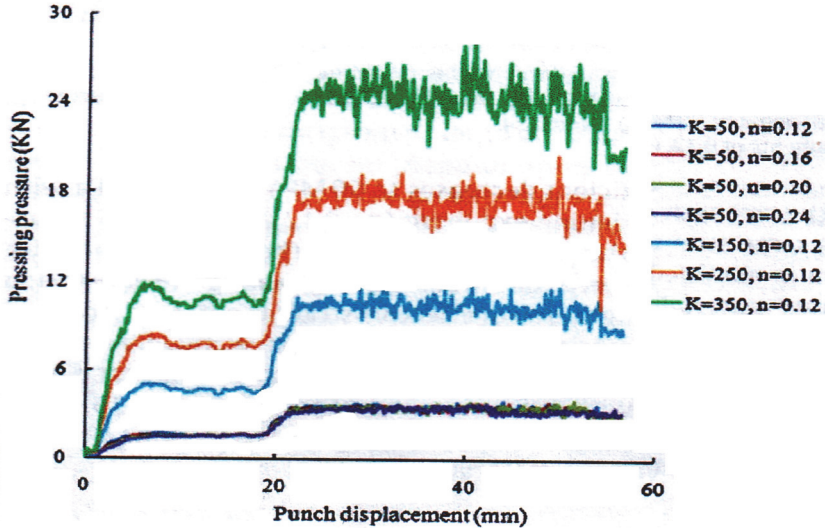


Figure 1.13 Diagram of magnitude of compressive pressure versus strain hardening exponent values [36].

Prediction of strain hardening and strength to generate value on the flow stress in ECAP consolidation and parallel channel has been studied in [35-38]. The first shift of pressing depends on the calibration of machine pressing, for example, strength magnitude remains constant at 50 MPa (as initial step pressing), every point on the pressing resulted in increased strain hardening. The resulting strain hardening exponents are: 0.12: 0.16: 0.2 and 0.24, which correlated with the magnitude of pressure. Figure 1.13 shows the relationship between the extents of compressive force during ECAP-PC to the value of the resulting strain hardening coefficient. The movement of the sample from the initial setting to the end is accompanied by the increase in strain value. Before reaching the second bend, a decline in the force was around 88%. When the magnitude of the strength decreases further from 350 MPa to 50 MPa as the first setting of the machine, as shown in Fig. 1.13, resulting from the strain hardening exponent ($n=0.12$), after the second corner, the cross section was reduced to 87% [35-36]. It can be assumed that if a copper capsule is used when consolidating composite powders, it does not impede the flow stress by twinning deformation, thus, the dislocation movement will be able to provide a more optimal flow stress.

1.5 Accumulative roll bonding (ARB)

ARB is a type of the SPD process where rolling a stacked sheet material is used to decrease the grain size. Generally, nanometer sub-micron or nanometer grains have higher strength than conventional materials that have grain sizes larger than a few tens of micrometers [39-40]. Stages of the ARB process are: cutting according to the size and capacity of the roll machine, stacking and rolling for several cycles. As compared to other SPD processes, ARB has the advantages, such as considerable force by capacity forming and the process itself is simple. Also, dies are not needed in the processes, therefore it has the ability for enormous productivity in mass numbers. The process is shown in Fig. 1.14. This process can be recommended for commercial and industrial applications [39-41].

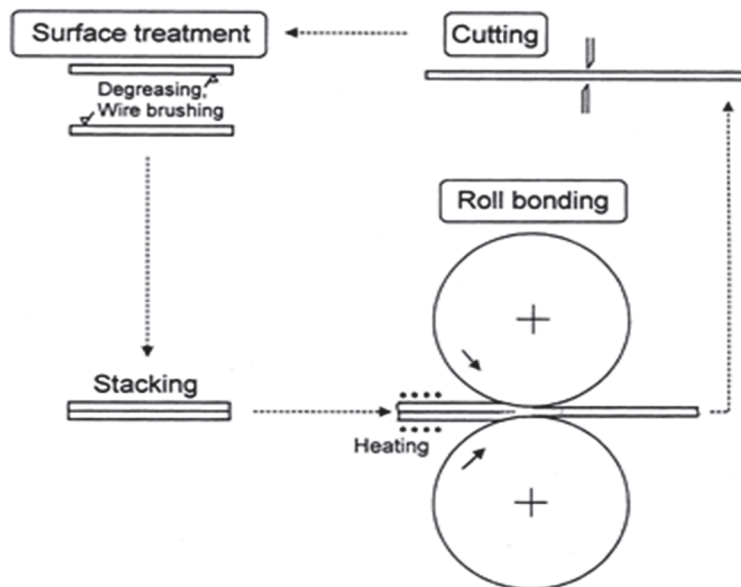


Figure 1.14 Stages of ARB process [40].

Formability of ARB

In order to create formability, the stages of the process must be done well. Temperature, speed rolling, work-piece thickness, roll diameter, which influence the process parameters, affect formability. Speed of rolling at high temperatures promote the strength of the bond between the layer material and will cause strain hardening. During deformation, temperatures and strain control the work process [42-44]. Formability is the most critical success factor material to be processed [42]. Temperature increases the formability, the use of temperature varies depending on the type of material or matrix used, and however, mainly the recrystallization temperature

is used. Use of temperature 100-450 °C is the upper limit for recrystallization for aluminum alloys, good for bonding and workability but leads to cancellation of strain accumulation. To produce good formability during the ARB process, to obtain high strain rate sensitivity, temperatures in the range of 300-350 °C must be used [45-46].

Interphase mechanism of ARB process

The formation of a bond interface is affected by the roll bonding process that results in cold welding, thus forming a bond between the metal layers participating. Sufficient compression to the appropriate temperature affect bond strength, which is able to improve mechanical properties. Consequently, strong welding between the layers becomes a benchmark for the strength of materials bonding [47]. Recrystallization temperature helps the formation of a material bond by the diffusion processes. The diffusion bonding will make the plate attachment firm. Bonding mechanism is shown at Fig. 1.15. There are stages of the formation of the bond between the plates that coupled during ARB. The brushing of the surface increases the total surface area, so that a stronger bond is formed between the two sheets [48].

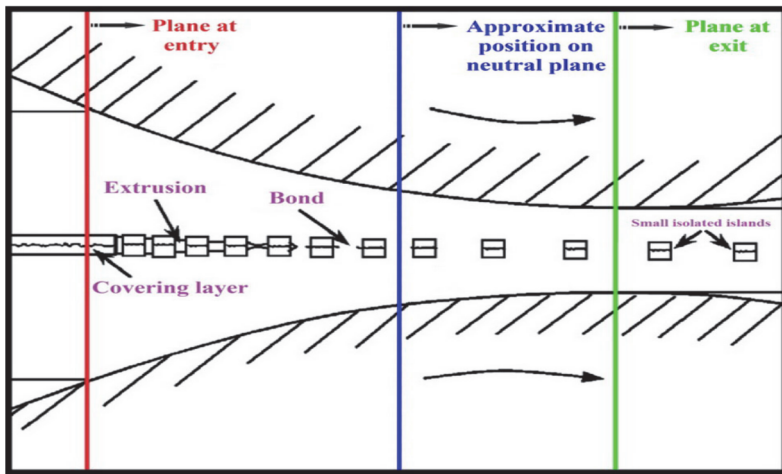


Figure 1.15 Bonding mechanisms during the ARB process at first cycle [48].

Evolution of microstructure during the ARB process

It was reported that during the ARB process shear strains build up excessively by friction between roll and sheets which improves the grain refinement [48]. There are two conditions in the process - if the samples are without lubrication, then the grains structure has parabolic profile in the thickness of the strips. This indicates that the highest level of compression has been achieved during the first cycle, which results in the formation of a single parabola distribution excessive in shear strain, thus indicating the peak shear strain on both surfaces. If samples are lubricated, it will

change the dependence on the position in the thickness of the couple of sheets and produce a short parabolic movement, as shown in Fig. 1.16 [49].

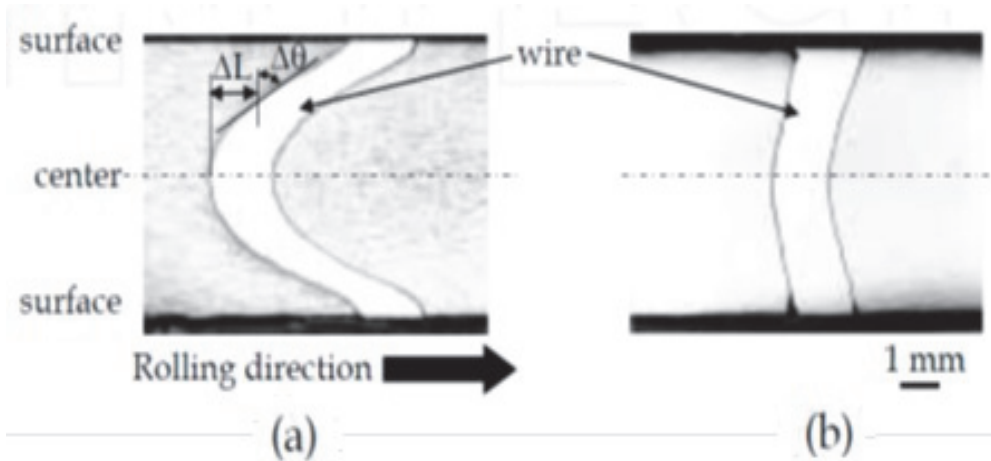


Figure 1.16 Embedded pin method of flection of wire in the couple of sheet after the rolling process: (a) sample without lubrication; (b) sample with lubrication [49].

Rolling process parameters affect the performance characteristics of the ARB: pressing rolls are the most important in parameter processes; furthermore, several process variables, such as up-down of roll diameter, materials reduction, velocity of roll, friction and metal flow conditions, affect the success of metal processing by ARB. The relationship is qualitatively equivalent to the shear deformation of the micro strain through the thickness of the sheet in the method of pin embedded, as shown in Fig. 1.16. It is commonly used to predict shear strain through the thickness of the experimental, the magnitude of shear strain and equivalent strain obtained in this method are a prediction. Therefore, to control the micro level, it is important to measure the deformation behavior on the sheet accurately and quantitatively through a combination of experimental rolling and finite element simulation. Shear strains are caused not only by the friction with the roll, but also by the surface texture and the diameter of the rolls. Variable Ld/td , Ld indicates the zone of the contact arc projection of horizontal plane, and td is the result of thickness of the sheet, shown in Fig. 1.17. The ratio Ld/td predicts the distribution of strain in the various friction conditions. Thus, it can be used to understand the deformation behavior, for example using methods of embedded pin on the ARB experiment with respect to some variable related [49-50].

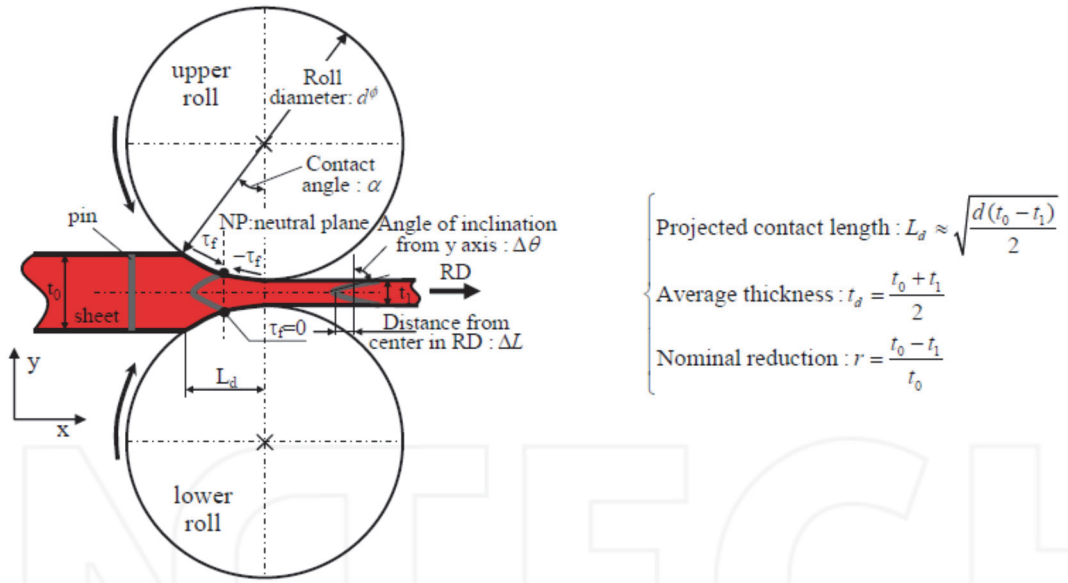


Figure 1.17 The geometry of the ARB process [49].

Grain size distribution, a reversal form of a parabolic shape in profile shear strain, caused a decrease of the width of grain in the central area of the sample cycles and UFG structure occurred in the area below the surface. For cutting, stacking and bonding rolls procedure, which severely sheared the layer on the first cycle that comes in the second cycle towards the middle layer thickness leads to a double parabolic curve. Then a set of coils was fixed in UFG in the center of the strip samples [50].

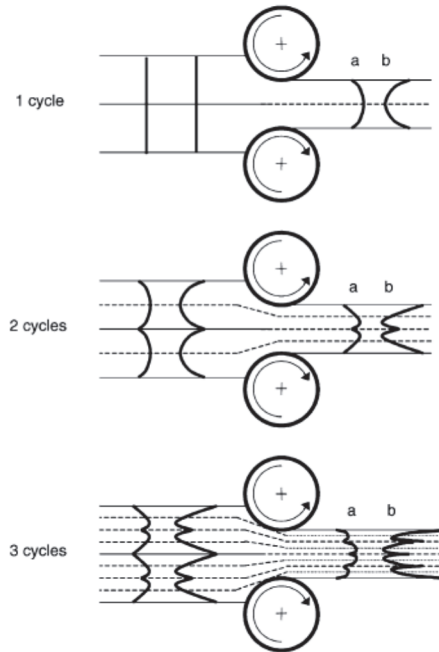


Figure 1.18 Schematic illustration of microstructure evolution: a - shear strain condition; b - strips during ARB process [50].

The friction between the roll and the surface of the material causes shear strain due to the contact zone and roll geometry, reduction of rolled is 50% with and without lubrication. When the roll contact dimension on strain action is not symmetrical, it will result in the non-appropriate roll bite geometry. It is a result of un-lubrication, otherwise by the lubrication process, the embedded-pin is less powerful, as shown in Fig. 1.16. Additional cycles on the ARB processes will produce elongated equiaxial grains resulting from strain hardening, as shown in Fig. 1.18. Each cycle then elongates the grains, which increases the hardness. Microstructure evolution during the ARB process and the processes in the interface bonding are the most important factors that determine the mechanical performance of the processed material [51-52].

Distribution of strains during the ARB process

The finite element method (FEM) was used to predict the strain and stress field during processing. The variables t_0 as initial thickness and l as length will be defined according to FEM analysis. Frictional condition among the speed of the roll sheets is expressed as $\tau_f = \mu p$, where τ_f is the shear stress, μ is the coefficient of friction and P is the pressure rolling. The Coulomb law for friction condition of pull sheets in the roll bite process sheets is referred to by $\mu > \tan \alpha$, as illustrated in the schematic of ARB variables in Fig. 1.17.

Von Misses is a classical plasticity theory, which is often called isotropic Plastic Hardening, reveals ε_{eq} , an equivalent strain imposed by rolling that is defined below:

$$\varepsilon_{eq} = \int_0^{t(steady)} \frac{d\varepsilon_{eq}}{dt} dt \quad (1.3)$$

To search for the incremental shear strain, the additional strain in the x direction can be found with the following equation, where: $d\varepsilon_{eq}/dt$ is the stages of equivalent strain, t (steady state) is the time of rolling, strain in the x direction, $d\varepsilon_{xx}/dt$.

$$\frac{d\varepsilon_{eq}}{dt} = \frac{2}{\sqrt{3}} \sqrt{\left(\frac{d\varepsilon_{xx}}{dt}\right)^2 + \frac{1}{4}\left(\frac{d\gamma_{xy}}{dt}\right)^2} \quad (1.4)$$

In eq. (1.5), $d\gamma_{xy}/dt$ is the gradual shear strain caused by the direction of shear stress τ_f . This equation defines the total shear strain as illustrated in Fig 1.17.

$$\gamma = \int_0^{t(NP)} \frac{d\gamma_{xy}}{dt} dt + \int_{t(NP)}^{t(steady)} \left| \frac{d\gamma_{xy}}{dt} \right| dt \quad (1.5)$$

The first condition is the positive shear strain which is induced by the shear stress, τ_f . The second condition is the negative shear strain γ , which represents the total magnitude of the shear strain γ_{xy} , this case regards deformation during ARB, during which $d\gamma_{xy}/dt=0$ and $d\varepsilon_{xx}$ are both constant during the processes [49].

It is assumed that with increased number of ARB process cycles, the bonding of the layers could become unstable. This instability can be caused by a dispersion of the reinforcements from surface area toward the interior of the composite, therefore buildup of strains during the processing and material becoming brittle [49-53].

1.6 Latest developments in SPD

During the last 15 years, the SPD methods have been developed rapidly. New methods simplify the process or enable producing materials with superior properties. Some examples of new developments in new SPD methods are presented in Fig 1.21. Development of new SPD methods is driven by the requirement of simplifying the process, so that it can be applied for mass production.

Type of SPD	Schematic Illustrations	Developed in
Equal Channel Angular Rolling		Korea Institute of Science and Technology (KAIST) KOREA (2001)
a. Multi Rolling Angular Extrusion b. Reversed shear spinning		Friedrich Alexander University of Erlangen-Nürnberg Martensstr GERMANY (2005)
Equal Channel Angular Torsion		Hefei University of Technology, Hefei CHINA (2008)
Continuous-High Pressure Torsion		Continuous Press-Torsion Kyushu University, JAPAN (2010)
Accumulative Press Bonding		Brunel University of London United Kingdom (2013)

<p>Accumulative Continuous Extrusion</p>		<p>Northeastern University Shenyang, CHINA (2015)</p>
<p>Repetitive Press-Roll Bonding</p>		<p>Tallinn University of Technology, ESTONIA [this work] (2016)</p>

Figure 1.21 Schematic representations of new methods of the SPD process.

In 2001, the Equal Channel Angular Rolling (ECAR) was developed, in 2005, two processes were renewed; Multi Rolling Angular Extrusion (MRAE) and Reversed Shear Spinning (RSS). In 2008 - 2010 Equal Channel Angular Torsion (ECAT) and Continuous-HPT were added [54-56] and in 2013, Accumulative Press Bonding (APB) [57] was created. The APB process requires 10-16 cycles to produce high mechanical properties. In 2015, new process named Accumulative Continuous Extrusion was developed [58] and in 2016, RPRB process was reported that combines uniaxial press and ARB processes. The pressing is performed without lubrication using a hydraulic or pneumatic machine.

1.7 Heat treatment of aluminum alloys

Precipitation strengthening of solid solution occurs due to the process of fine grained dispersed precipitates during aging, it can happen on two conditions: artificial aging (AA) and natural aging (NA). Super saturation zone formation will be faster in the presence of diffusion in the deposition conditions, the diffusion coefficient of equilibrium will result in the first saturated solid solution which is a cluster of solute, followed by the establishment of the transitional non-equilibrium deposition [59].

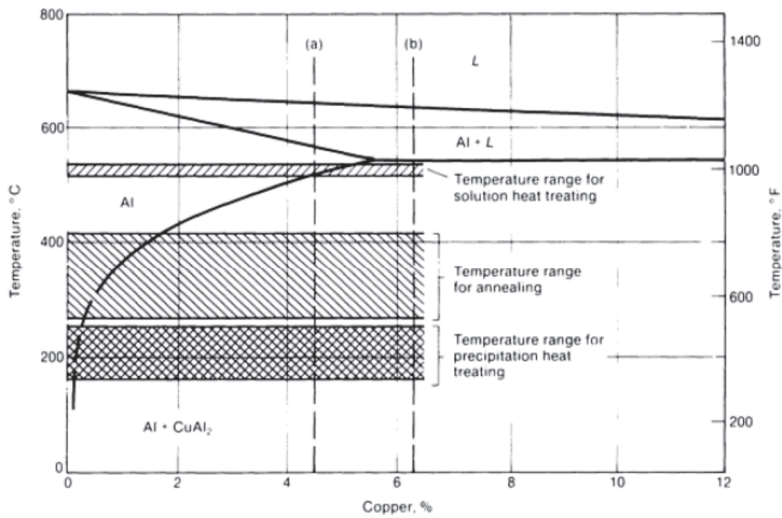


Figure 1.22 Binary phase diagram (up to 12 % Cu) and temperature ranges for heat treatment at 5.65 wt % Cu [59].

The temperature ranges for precipitation in aluminum-copper alloys are schematically shown in Fig. 1.22, illustrating the required solubility-temperature relationship needed in precipitation strengthening. It shows the temperature ranges required for solution treatment and subsequent precipitate hardening in the aluminum-copper system. The equilibrium of solid solubility for Al-Cu as temperature increases from about 0.20% at 250 °C to a maximum of 5.65% at the eutectic melting temperature of 548 °C. (It is considerably lower than 0.20% at temperatures below 250 °C) for aluminum copper alloys containing from 0.2 to 5.6% Cu, two distinct equilibrium solid states are possible. At temperatures above the lower curve in Fig. 1.23 (solvus), copper will be soluble, when the alloy at this temperature has enough time to diffuse the copper fully into the solution. At temperatures below the solvus, at the equilibrium condition, there are two solid phases: solid solution, α , an intermetallic-compound Al_2Cu as phase θ [59].

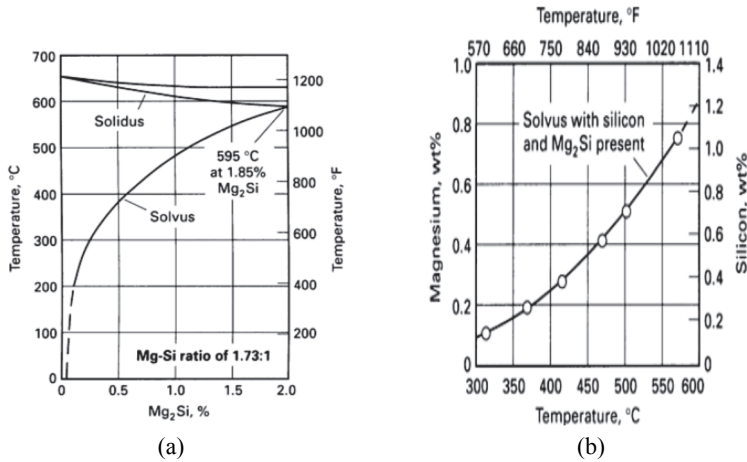


Figure 1.23 Function of temperature for the solubility equilibrium: (a) Mg_2Si in Al-Alloys with Mg-Si ratio of 1.73 to 1; (b) Mg and Si in solid condition when both Mg_2Si [59].

Some commercial alloys can be improved by the heating of several series of Aluminum, such as; 2xxx, 6xxx, and 7xxx as wrought alloys (except 7072) and 2xx.0, 3xx.0, and 7xx.0 series casting alloys, between other elements like Cu or Cu and Si as the primary strengthening alloy addition. In the heat treatable alloys, there are combinations with such elements as: Cu, Si and Zn, some Mg with other elements capable of accelerating precipitation hardening, 6XXX series alloys containing Si and Mg (Mg_2Si). AA2xxx and 7XXX is the strongest, but AA6XXX has the best formability among others, enabling the application of the manufacturing series 6 that is widely used [59]. Aluminum alloy 6061 is widely used for structural applications, also in the automotive industry [60-61]. AA7075 is a precipitation hardened alloy, widely used in the aerospace and automobile industries. Still, AA7075 has limited formability. It is conventionally produced by forging at elevated temperatures [62-63].

Strengthening mechanism of aluminum composite by the SPD process

An aluminum based composite was developed to substitute materials for steel and cast iron. Alumina is considered as reinforcement suitable for aluminum as a matrix due to its availability and low cost compared to other ceramic materials, such as; SiC, ZrC, TiB_2 , and carbon. Besides that, the hardness of composites containing Al_2O_3 is higher than other reinforcements. In the composite material Al_2O_3 as reinforcement it can inhibit grain growth also to increase the hardness although it reduces densification. Based on this phenomenon, the SPD is suitable for the fabrication process of composite Al/ Al_2O_3 for bars or powder based composite materials, process by ECAP [23-24] and form of the sheet process by ARB [10]. Fine grain size will affect the evolution of the microstructure, which will improve the mechanical properties, so that the value of shear strain will also increase. The processing

parameters of ECAP have the specific features to enable formation of the work-piece rod or powder for ARB application on the sheets, as in Fig. 1.24; process of ECAP and ARB will result in high strains for metal caused UFG [64]. The grain size affects the mechanical behavior for materials design that has superior mechanical properties enabling control of the grain size; furthermore, the grain refinement is the method for improvement of mechanical properties: strength and hardness without sacrifice of ductility and flow properties [65-70]. This condition can be expressed with the formula of Hall-Petch where the smaller the particle, the higher strength:

$$\sigma_y = \sigma_o + k_y \cdot d^{-1/2} \quad (1.6)$$

Where grain size is d , σ_y is yield strength, σ_o represents friction stress and k_y is a constant. Decreasing the grain size increases the strength of materials. This has attracted interest among scientists and industry to pursue the SPD processes.

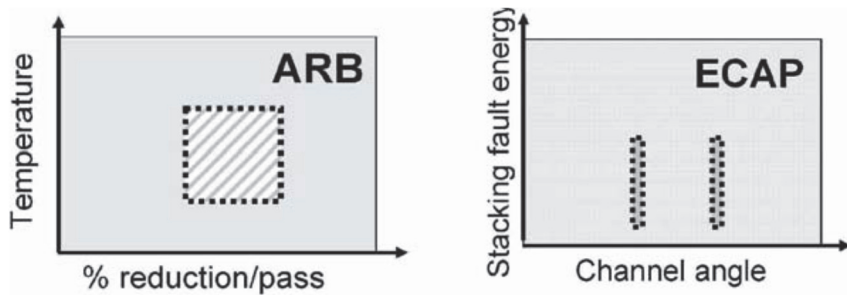


Figure 1.24 Processing parameter domains for ARB and ECAP [60].

To refine grain size of commercial alloys, thermo-mechanical treatment is necessary. The applied temperature must be sufficient to provide formability, but must be kept below crystallization temperature to inhibit grain growth due to diffusion [24, 71].

1.8 Main objectives of the thesis

A motivation of this study was limited development of the SPD methods to consolidate MMCs. Almost all of the regimes and rules of the SPD process, such as ECAP and ARB, are applied for metal alloys. Determination of consolidation of aluminum alloys powder as the composite matrix is an important variable to consider first, before the development of the technological routes for MMCs. Heat treatment regimes cannot be derived from those of standard aluminum alloys, as an additional mechanism to grain size, the overall mechanical properties will affect. The dependence of mechanical properties (strength and ductility) on simultaneous effect from grain growth and formation of dispersoids must be ascertained. The help of FEM will simplify the determination of the phenomenon in the SPD process, such as the

effect of temperature of pressing, which contributes to the formation of fine grains during SPD processes.

Another important goal of this research is to produce a composite material where ceramic nanofibers are aligned in aluminum matrix by SPD processes. ECAP and ARB are among SPD technologies that are more applicable, therefore study will focus on development of these.

The weakness of the ECAP and ARB is the long processing time due to a large number of passes needed to produce optimal properties; therefore the novel process of RPRB will be presented, overcoming this weakness.

The main objectives of the research are:

- To develop the most applicable SPD processes and parameters to effectively compact aluminum alloy powders and ceramic MMCs reinforced by 2D nanostructures;
- To assess the microstructure-property relationships for MMCs reinforced with aligned ceramic nanofibers;
- To develop SPD methods to reduce cycle times when compacting MMCs. Material yield, sample integrity and processing time are under study for a possibility of industrialisation

The main activities in this research are:

- To identify the processing characteristics of AA1070, AA6061 and AA7075 by the ECAP compaction process to obtain baseline matrix for the composites;
- To produce aluminum composite materials with Al_2O_3 nanofibers as reinforcement using SPD methods;
- To develop RPRB as a novel process to decrease the number of cycles.

2. EXPERIMENTAL PROCEDURES AND MATERIALS

2.1 Materials

2.1.1 Materials for ECAP and ECAP-PC

The materials used as matrix were AA1070, AA6061, AA7075 powders with particle size 70-100 μm , received from Aluminum Powder Company Ltd. The alumina nanofibers (γ -ANF) had particle size in the range of 7 nm and length of about 50 μm . The nanofibers were aligned in blocks with dimensions of about 100x100x50 mm.

Table 2.1 The chemical composition of aluminum alloys, wt.%

Al alloys	Al	Si	Fe	Cu	Ti	Cr	Zn	Mn	Mg	V
AA1070	99.7	0.20	0.25	0.04	0.03	-	0.04	0.03	0.03	0.05
AA6061	97.13	0.76	0.7	0.22	0.1	0.07	0.06	0.04	0.92	-
AA7075	89.76	0.052	0.19	1.59	0.025	0.19	5.68	0.007	2.51	-

2.1.2 Materials for ARB and RPRB

AA1070 (sheet size 50 \times 400 mm and thickness of 3 mm) and AA7075 (sheet size 50 \times 270 mm with a thickness of 14 mm) were used as the matrix starting material. As the reinforcement 0.4 wt. % ANF were added, cut out as thin sheets from the blocks, perpendicularly to the length of the fibers.

2.2 Ball milling process of aluminum powder based composite

Aluminum alloy powders and ANF mixture were mechanically mixed by wet ball milling in a tumbling mill. The amount of ANF in the aluminum alloy (1070 and 6061) matrix was 3 wt. %. Milling was performed in ethanol at 60 rpm for 24 hours. Ball to powder ratio 1:10 was used in 500 ml hard-metal lined vessel.

Mixing powdered matrix and reinforcement are a critical step in order to achieve homogeneous distribution of reinforcements throughout of the composite material [70-72]. The horizontal ball mill, as shown in Fig 2.1, can produce moderate quantities of material in moderate milling times.

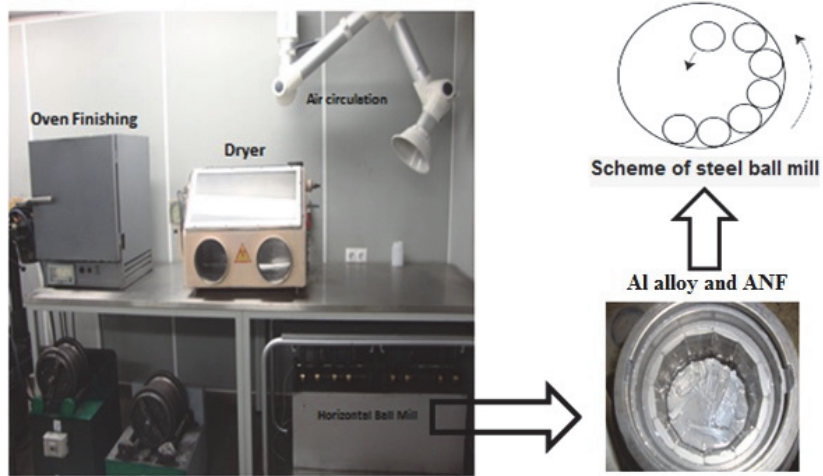


Figure 2.1 Device of horizontal ball mill process.

2.3 ECAP methods and processes

Aluminum alloy powder was wrapped in a copper sheet and heated in a resistance furnace at 400 °C with a holding time of one hour. The samples were pressed on one pass, the range of pressing 400-500 MPa at the rate of 5mm/s on 16×16 mm square through the corner of the dies 90° whereas graphite was used as lubrication.

For parallel channel-ECAP, two shearing events occur, sample sliding in two subsequent deformation zones. The value of the displacement between the two parallel channels, deformed zone, and the corner of the intersection of two channels, are the main parameters of die geometry which affect both the pattern of flow and strain-stress state during the ECAP-PC process.

Description of the process is presented in Fig. 2.2.

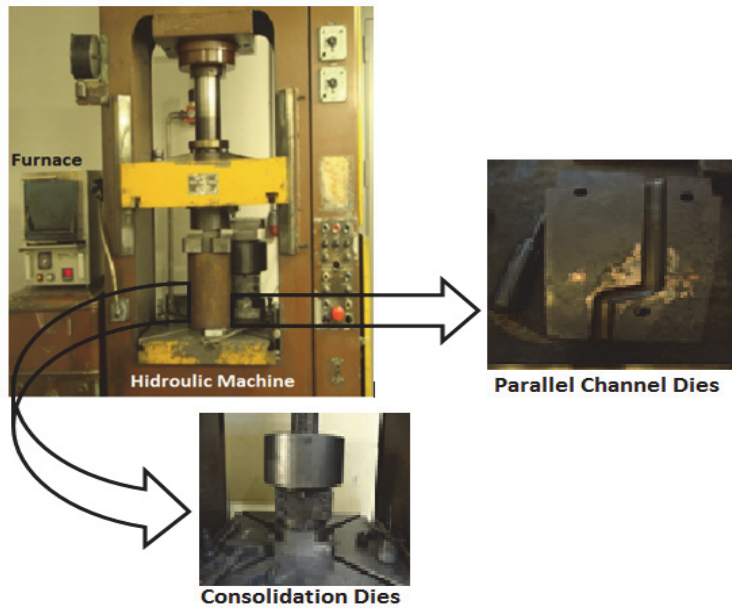


Figure 2.2 Machine and tools for ECAP.

2.4 Heat treatment

Aluminum alloy 6061

Heat treatment was performed to find its influence on the highly strained UFG alloys and composites. Annealing of AA6061 was conducted by heating the sample up to 415 °C and holding for 2.5 hours. Then the temperature was lowered to 177 °C and held for 8 hours. Solution heat treatment (T6) was performed by first holding at 530 °C for 1 hour, quenching and then holding at the temperature of 100 °C for 1 day, as shown in Fig 2.3.

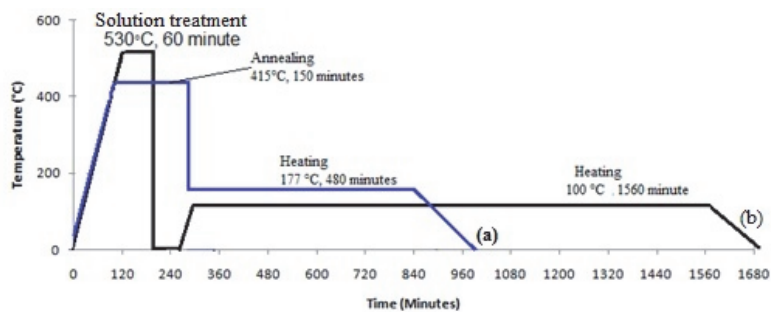


Figure 2.3 Diagrams of heat treatment for AA6061: (a) annealing-(O); (b) solid solution treatment (quenching + artificial aging)-(T6).

Aluminum alloy 7075

Annealing of AA7075 was conducted by heating the sample up to a temperature of 415 °C and holding for 2 hours. Then the temperature was lowered to 230 °C and held for 4 hours. T6 heat treatment was done first by solution heat treatment at 500 °C for 1 hour, quenching and then holding at the temperature of 120 °C, as shown in Fig 2.4.

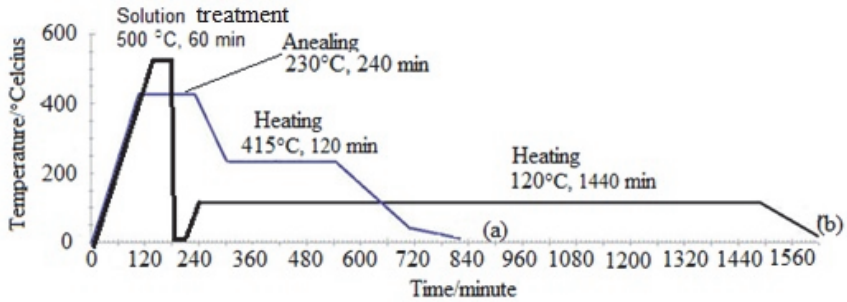


Figure 2.4 Diagrams of heat treatment for AA7075: (a) Annealing-(O); (b) Solid solution treatment (Quenching + artificial ageing)-(T6).

2.5 Accumulative roll bonding (ARB) process

The ARB process was carried out with no lubrication, using a rolling mill with a loading capacity of 60 tons and rotation speed of 50 rpm. Reduction of 50 % during each pass was used. After the first rolling, the bonded strips were cut in half and heated above the recrystallization temperature at 450 °C. The process is shown in Fig. 2.5. For roll bonding of AA1070 laboratory rolling mill with a diameter of 150 mm was used; the length of the roll being 180 mm.

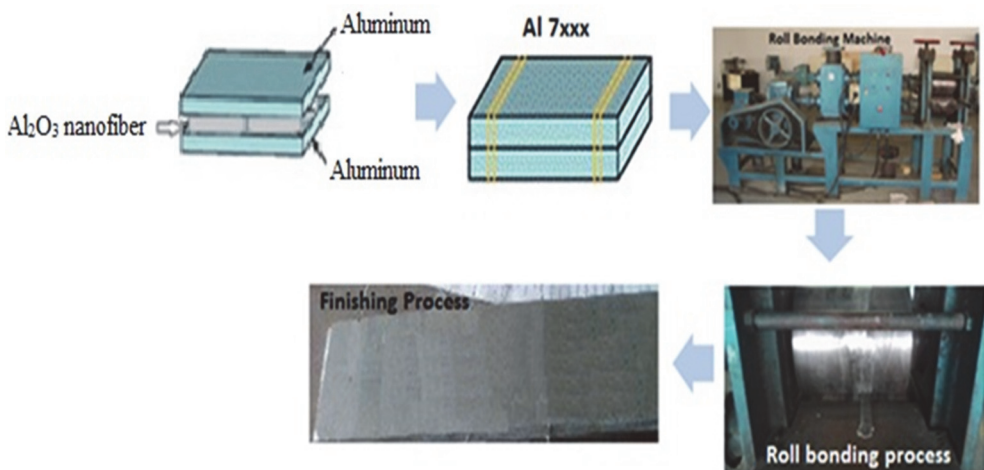


Figure 2.5 ARB Process

2.6 Repetitive press roll bonding (RPRB) process

By RPRB process, pressing in open die was added to the standard ARB, prior rolling cycle, as shown in Fig. 2.6. The first uniaxial-pressing was carried out with no lubrication, using a 500 ton hydraulic press. The pressing was stopped when 50% of the reduction was achieved. Thereafter, the bonded strips were heated at the recrystallization temperature at 400 °C for holding time of 1 hour. During the second step, 50% of the reduction by rolling was performed on strips preheated to the temperature of 350 °C.

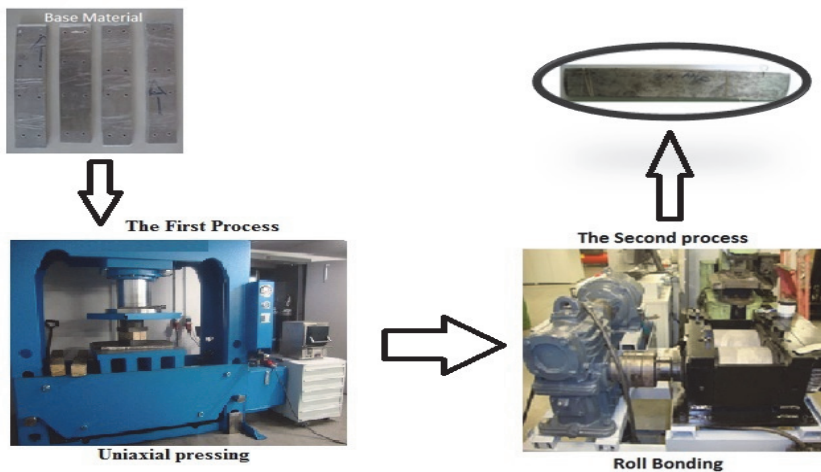


Figure 2.6 RPRB process.

2.7 Study of microstructure and properties

Microstructure was studied by means of Scanning Electron Microscopy (SEM) using microscopes JSM-6510LA by JEOL and TM-1000 by Hitachi. Image-J software was used for quantitative microstructure analysis. X-ray Diffraction (XRD) measurements were performed by Zeiss EVO MA10 to determine phase composition of the composites. Hardness of the compacted alloys and composites was measured by the Vickers Hardness method (HV10). Servo-hydraulic testing machine Instron 8516 was used for quasistatic compressive strength tests, measured on cylindrical ECAP and PC-ECAP specimens. Tensile testing measurements were performed for ARB and RPRB samples. To explore the variable effect of pressure and temperature distribution on the materials during the processing, Finite Element Methods (FEM) analysis was used with R14.5 ANSYS software.

3. RESULTS AND DISCUSSION

3.1 Aluminum Alloys by ECAP Consolidation

3.1.1 Microstructure

Heat treatment was performed on ECAP consolidated aluminum alloys. To improve the ductility, annealing process (O) was used. To study the effect of grain growth and formation of precipitates, solid solution (T6) was applied. As it follows from the microstructure, matrix phase aluminum grains are distributed between Mg_2Si precipitates (see Fig 3.1(a)). After ECAP processing (without heat treatment), the aluminum alloy 6061 has a grain of $0.19\ \mu m$. Ferrasse, et al. [73] produced UFG 6061 alloy by using ECAP as post processing of AA 6061 billet, reaching an average grain size down to $0.2\ \mu m$. Figure 3.1 (b) shows the distribution of Mg_2Si after annealing. Average grain size reaches $8.9\ \mu m$ with the formation of grains and precipitation located at grain boundaries. Rao [74] showed the annealing at high temperatures resulting in precipitation which will stabilize the microstructure. The microstructure after solid solution treatment of AA6061 is shown in Fig 3.1 (c). Matrix grains have an average particle size of $1.3\ \mu m$.

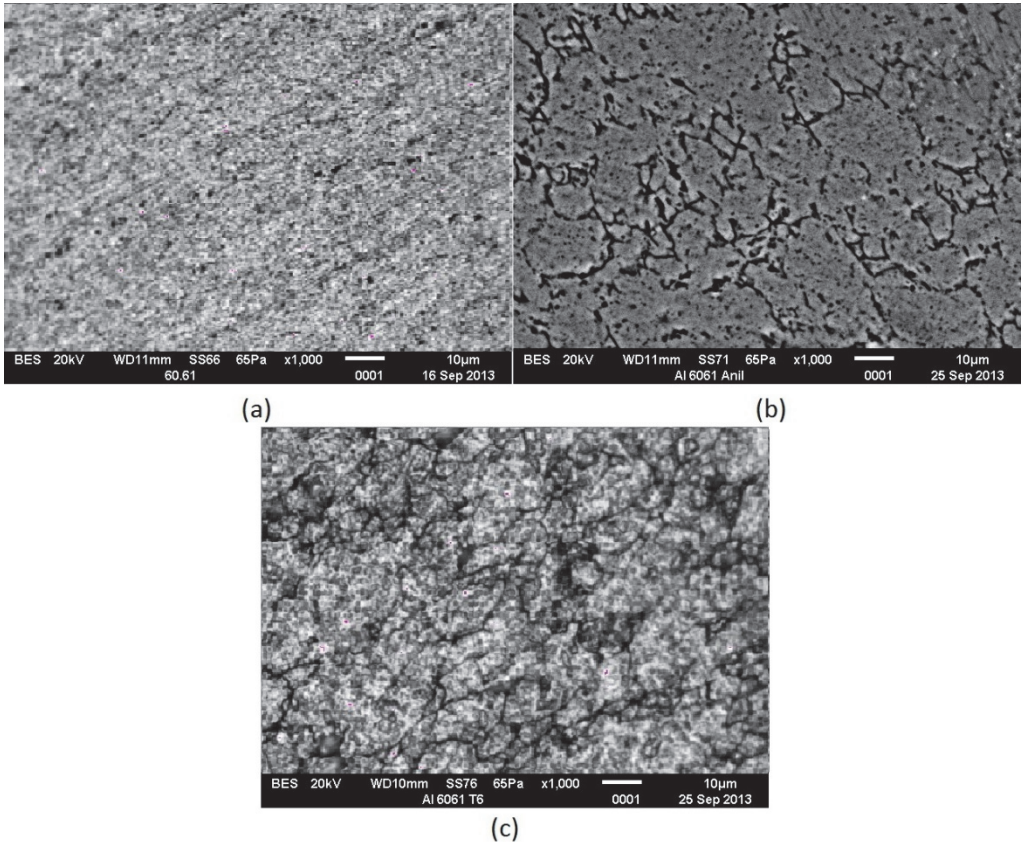


Figure 3.1 Microstructures of AA6061 by ECAP Consolidation: (a) AA6061 as ECAP without heat treatment; (b) AA6061 Annealed (O); (c) AA6061 after solid solution treatment (T6).

Heating to 530 °C dissolves all precipitates. Precipitation of the second phase has a significant influence on microstructural stability by pinning and also impeding the grain boundary motion. The presence of the second phase particles in a solution heat treated alloy shows increased thermal stability to UFG produced by ECAP consolidation. This can be caused by the presence of the second phase precipitates and also by oxygen inclusion, mixed into the material from native oxygen layer from the surface of the compacted particles.

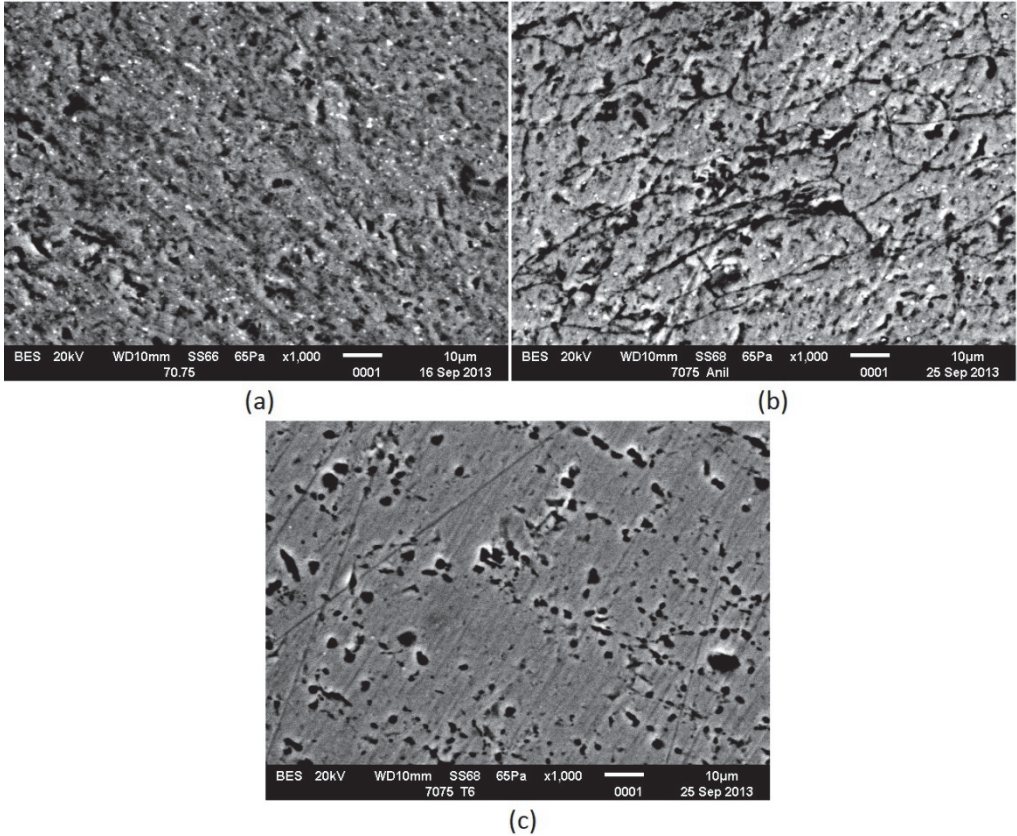


Figure 3.2 Microstructures of AA7075 by ECAP Consolidation: (a) AA7075 as ECAP without heat treatment; (b) AA7075 Annealed (O); (c) AA7075 Solid solution treatment (T6).

After annealing of AA7075, some segregation of the precipitates can be observed, which is accompanied by grain coarsening. This result is in accordance with [75-76], where the formation of large grains after over aging treatment is shown. These were elongated and flattened parallel to the rolling direction. Solution heat treatment with artificial aging (T6) leads to evenly distributed fine precipitates. Consolidated AA7075 has an average grain size of 0.75 μm . After annealing, the grain size increases up to 4.6 μm . Artificial aging yielded grain size of 4.4 μm . Annealing and solid solution eliminate micro-segregation of MgZn_2 , therefore the precipitate phase uniformly distributes in the aluminum matrix. Figure 3.2 shows micro segregation spreading evenly among the AA7075 matrix. This phenomenon results in grain coarsening and therefore decreases in hardness.

To investigate precipitation formation in AA6061 and AA7075, an XRD test was used. Formation of Mg_2Si precipitate in AA6061 occurred after solutionizing and

artificial aging, as evidenced in Fig 3.3 (a). The identified peaks for $MgZn_2$ precipitates in AA7075 can be seen in Fig 3.3 (b). Precipitation of $MgZn_2$ in AA7075 yields the highest mechanical properties among the existing aluminum alloys but has a limitation of formability due to the nature of micro-segregation.

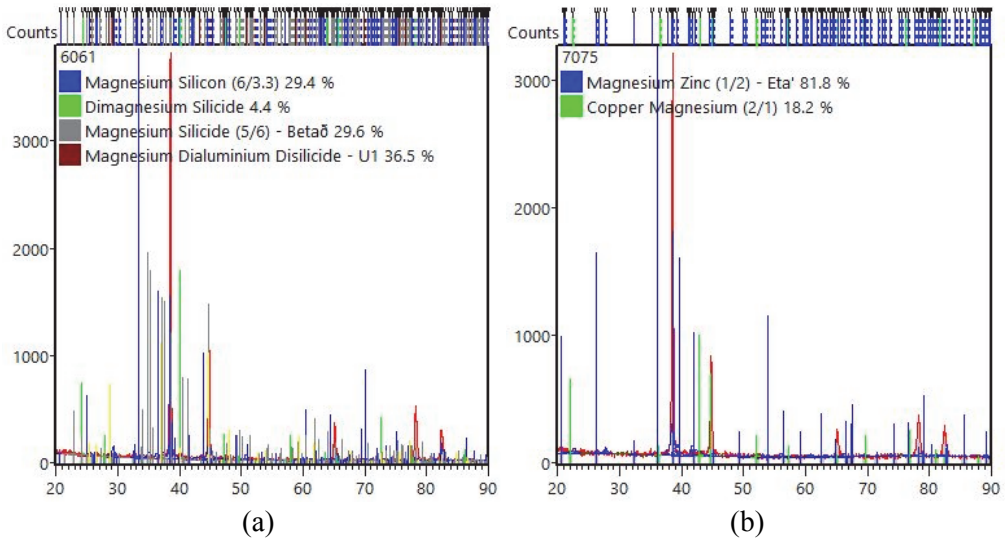


Figure 3.3 XRD results for precipitation of aluminum alloys: (a) Mg_2Si precipitated as the second phase of AA6061; (b) $MgZn_2$ precipitated as the second phase of AA7075.

ECAP consolidation is performed to determine the behavior of each alloy for further use of these with Al_2O_3 nanofibers as reinforcement. In continuation, AA6061 is consolidated by the process of Equal Parallel Channel Angular Pressing and AA7075 is used as a matrix in the Accumulative Roll Bonding process. Based on the literature, aluminum alloys (AA6061 and AA7075) are both suitable for application as a matrix phase in metal matrix composites.

3.1.2 Mechanical Properties

Hardness of ECAP consolidated materials is presented in Table 3.1. The hardnesses of as consolidated samples are 141 HV10 and 121 HV10 for 6061 and 7075, respectively. Simultaneous to densification, ECAP consolidation produces fine grains, increasing the hardness of the alloys. Simple shear during ECAP will result in high internal stresses so that grains are fragmented and distorted. Increase in hardness is directly proportional with compressive strength, shown in Figs. 3.4 and 3.5, compressive strength of 250 MPa and 395 MPa were measured for alloys 6061 and 7075, respectively. Annealing process improves ductility, but decreases drastically the hardness and compressive strength, and can be directly linked to grain coarsening.

The average grain size of AA6061 is 8.9 μm and grain size of AA7075 is 4.6 μm . Annealing yields in grain coarsening due to the diffusion processes. Solid solution treatment (T6) improves hardness and compressive strength. Hardness after T6 thermal treatment is 128 HV10 for 6061 and 105 HV10 for 7075. Compressive strengths of the materials are accordingly 225 MPa and 283 MPa. During T6 heat treatment, grain coarsening is levelled by the formation of fine precipitates, therefore producing increased mechanical properties. When compared to as compacted materials (ECAP without heat treatment), for alloy 7075, the ductility of the samples is increased. This indicates a possibility of effective use of ECAP consolidation also for aluminum alloys difficult to form if optimized post processing is used [77-79]. By annealing, recovery and recrystallization occurs, resulting in grain coarsening and aluminum becoming ductile. Solid solution T6 heat treatment increases the strength of the alloys, which is related to a finer structure and formation of precipitates.

Table 3.1 Mechanical properties of ECAP consolidated alloys

Alloy and Heat Treatment	Hardness HV10	Compressive Strength (MPa)	Deformation (%)	Grain Size (μm)
AA6061-ECAP	141 \pm 5	250	25	0.1
AA6061-O	88 \pm 1	97	45	8.9
AA6061-T6	128 \pm 3	225	29	1.3
AA7075-ECAP	121 \pm 4	395	2.5	0.7
AA7075-O	99 \pm 2	226	14	4.6
AA7075-T6	105 \pm 4	283	18	4.4

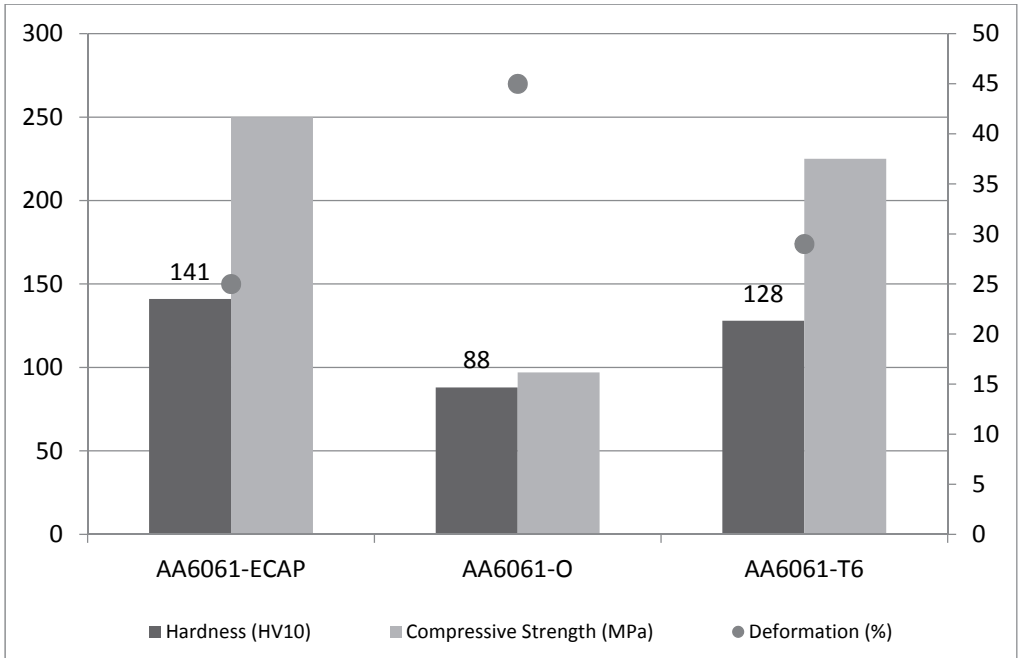


Figure 3.4 Mechanical properties of ECAP consolidated and heat treated AA6061.

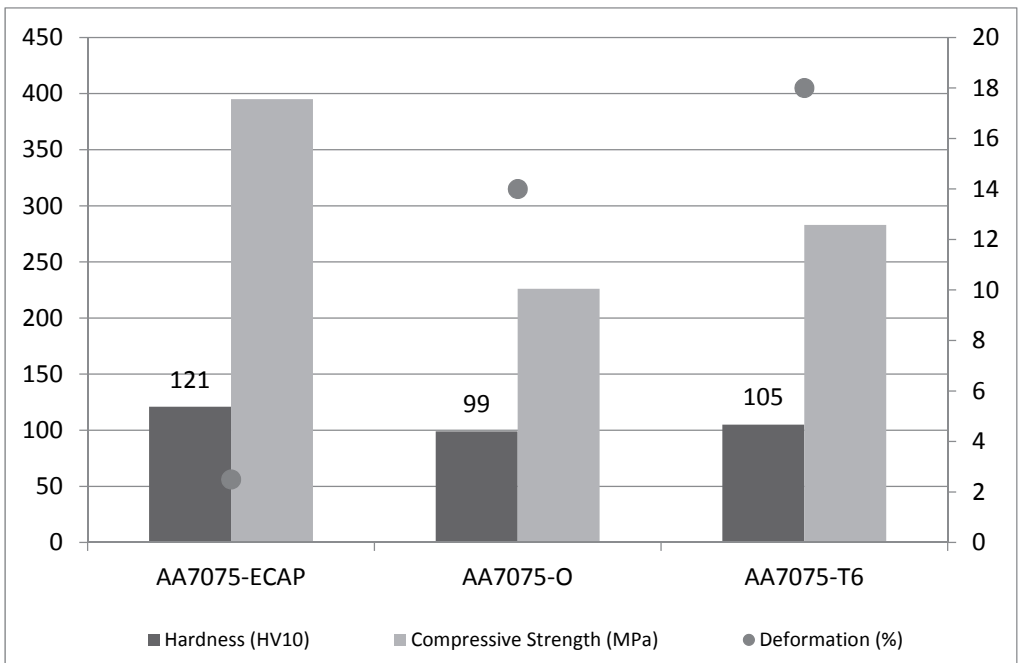


Figure 3.5 Mechanical properties of ECAP consolidated and heat treated AA7075.

3.2 Aluminum based composite by ECAP-PC consolidation

3.2.1 Microstructure

Cold pressing of aluminum alloys and composites by Parallel Channel-ECAP is expected to enhance formability and decrease waste when a high number of passes is used. Referring to [80], the process of consolidation at room temperature is preferred because of no need for extra step of preheating and higher effectiveness for grain refinement. However, as Fig. 3.6 (a) and (b) show, during cold pressing of AA1070 and AA6061 insufficient consolidation has appeared. Figure 3.7 shows that the distribution of stress is uniform: there is no heat flow on the samples, strain accumulation occurs along the copper capsule and dies interphase, resulting in micro-cracks.

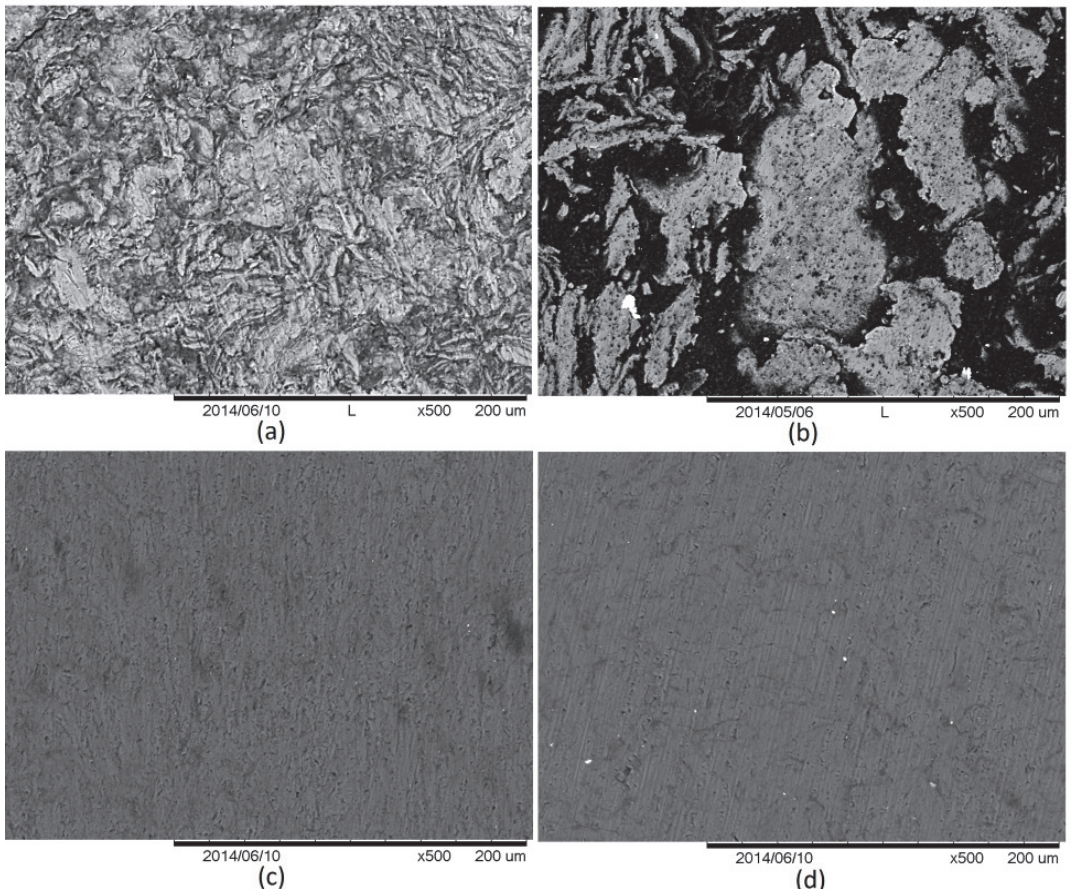


Figure 3.6 Microstructure of ECAP-PC compacted aluminum composite: (a) cold pressed AA1070; (b) cold pressed AA6061; (c) hot pressed AA1070 (d) hot pressed AA6061.

The deformation mechanism of ECAP-PC has been explained by twinning [80-81]. ECAP-PC defects originate from cracking and fragmentation which are considered as local mechanisms. As the Al/ANF powder was wrapped in Cu, the result was friction contact for the difference in materials flow, consequently blocking adhesion, causing micro-cracks shown in Fig 3.7 (a). At hot pressing (HP), the flow of stress is more easily moved toward the center point but still not evenly distributed. By hot pressing, micro-cracks do not occur, and high densification is obtained, as seen in Fig 3.6 (c) and (d). During the first pass, there is a possibility of grain morphology changes due to the mechanism of twinning, which decreases the local stresses at the grain boundaries. According Valiev et al. [34], ECAP-PC on the first pass twinning mechanism is not maximized, after four passes, the twinning movement is maximized, resulting in a homogeneous UFG material. With four passes, Mg₂Si precipitation is evenly dispersed. ECAP-PC makes it possible to produce a homogeneous UFG structure after four passes, which is a substantially smaller number when compared to conventional ECAP [77]. As it follows from Figure 3.8 (b), heat flow moved from the upper to the lower end, which resulted in stress and strains flow from the circle of the Cu capsule around the edges (Fig 3.8 (c)), as can be observed in Fig 3.8 (a), which explains no micro-crack around grains.

3.2.2 Mechanical properties

When copper capsule is used for wrapping powders, the copper reduces the friction coefficient, e.g. reducing the hydrostatic pressure from the surface to the center [82-83]. Pressure reduction is shown by ANSYS in Fig. 3.7. During cold pressing, stresses are gathered in the center and unevenly distributed. Although the flow pressure is higher when compared to cold pressing, flow pressure is still concentrated on the wall of the die, as seen in Fig. 3.8. Effects of die channel angle on the deformation behavior and increase of pressure on the punch die angle can result in increasing strain homogeneity in the cross-section [35]. Liu et al. [37] declared that during ECAP by parallel channels, the originally equiaxed grains are elongated after passing through the first bend, then returned to their original shape at the end the pressing. The largest flow stress of ECAP-PC occurred on the friction part of sides with dies [83-84] confirmed on HP in Fig. 3.8 (c). Deformation is localized in a small area around the meeting corner channel and material flow easily in the outer corner. This proves that the friction of powder inside the capsule Cu on the samples is very low in CP, thus, it cannot produce an optimum of mechanical properties.

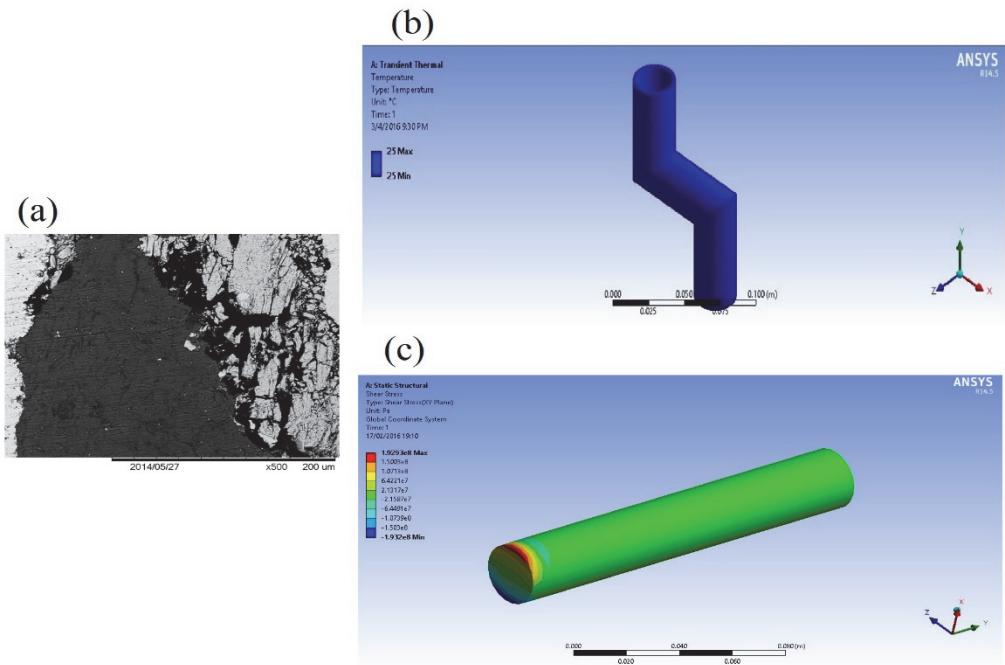


Figure 3.7 FEM simulation: (a) Microstructure after cold pressing; (b) effect of room temperature; (c) effect of cold pressing.

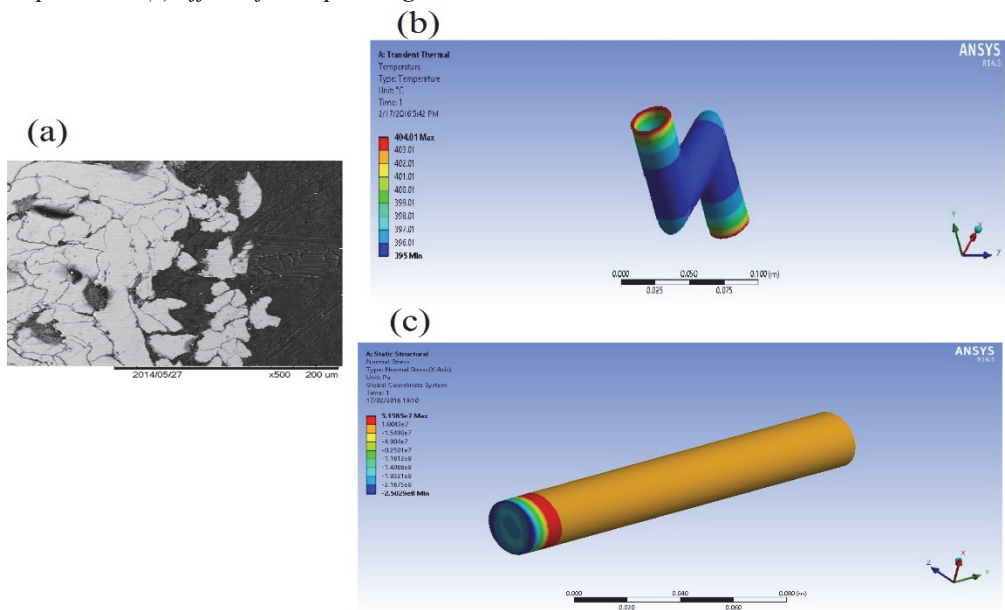


Figure 3.8 FEM simulation: (a) microstructure after hot pressing at the the Cu capsule – sample interphase; (b) effect of hot temperatures; (c) effect of hot pressing.

Hardness of AA1070 after cold pressing is 30 HV10, after hot pressing hardness increases up to 69 HV10. In cold pressing; compressive strength is 124 MPa and deformation 3% as compared with hot pressing, which reached 54 MPa and deformation of 14.5 %. This result is in accordance with measured grain sizes, being 5.7 μm for cold pressed materials and 7.5 μm for hot pressed materials. No UFG structure was present with ECAP-PC, which is believed to be caused by the lower level of applied deformations. Part of the deformation could also be accumulated in the Cu capsule around the specimen. Hardness for cold pressed 6061 alloy was 74 HV10 and for hot pressed alloys 95 HV10, as shown in Table 3.2. The compressive strength for cold pressed specimen is 57 MPa and deformation 2.4%, increasing up to 95 MPa and deformation of 14% with hot pressing. Although the hot pressing produces higher mechanical properties than cold pressing, the grains size in both cases is relatively coarse, i.e. 7.5 μm and 6.4 μm . Stress-strain behavior of AA1070 and AA6061 samples prepared by ECAP-PC shows the saturation trend, e.g. it does not show sufficient work hardening. If the strains during pressing are not sufficient to produce ultrafine grains, the mechanisms of formation of slip bands and twinning will not dominate. Therefore, unique mechanical properties cannot be obtained, shown by the tensile or compressive test. Mg_2Si precipitates, such as UFG structure formation, are accompanied by dynamic aging on ECAP-PC through four passes.

Table 3.2 Mechanical properties of ECAP-PC pressed nanocomposites

Composites	Hardness HV10	Compressive Strength (MPa)	Deformation (%)	Grain Size (μm)
CP AA1070 + ANF	30 \pm 3	124	3	5.7
HP AA1070 + ANF	69 \pm 5	73	14.5	7.6
CP AA6061 + ANF	74 \pm 5	57	2.4	7.5
HP AA6061 + ANF	95 \pm 2	95	14	6.4

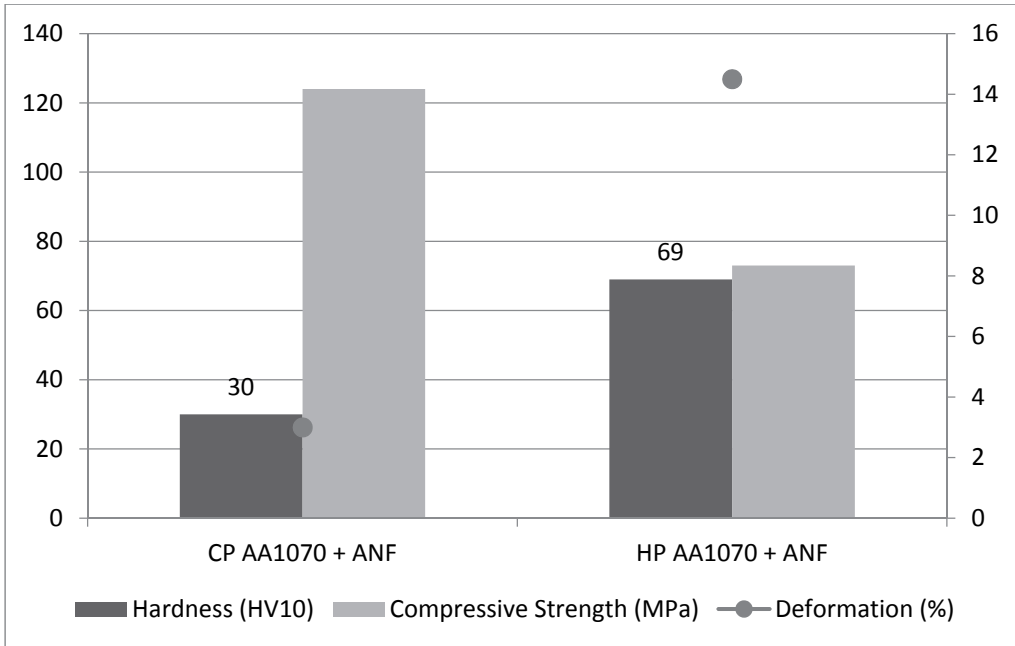


Figure 3.9 Mechanical properties of AA1070 compacted by ECAP-PC.

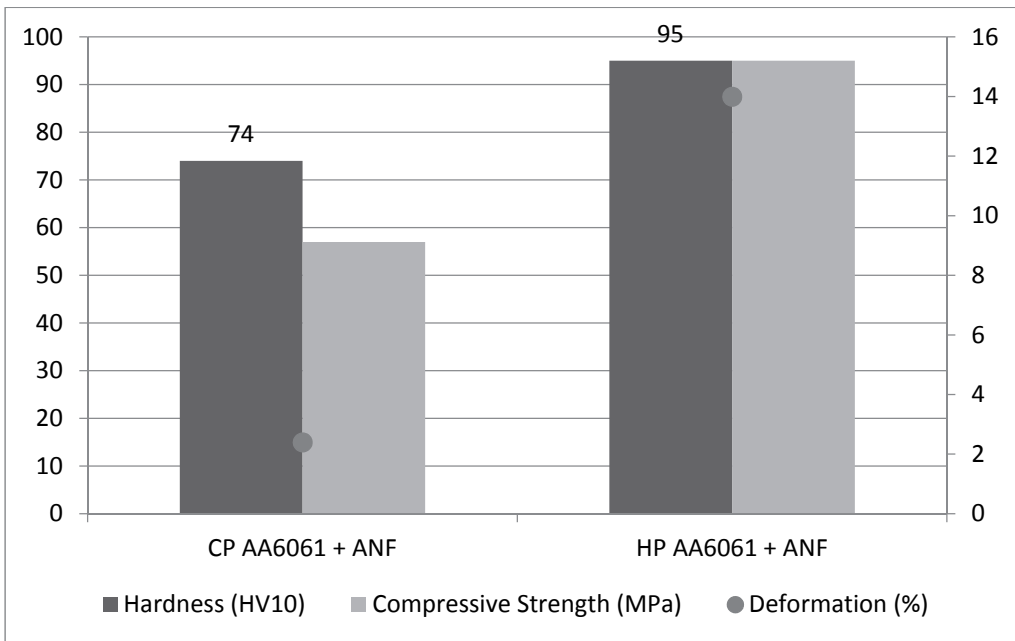


Figure 3.10 Mechanical properties of AA6061 compacted by ECAP-PC.

3.3 Aluminum based composites by ARB

For ARB, two different types of matrixes, i.e. AA1070 and AA7075 and Al_2O_3 nanofibers as reinforcement were used. Focus was on the observation of temperature effect during compaction. Cooling of the preheated strip was assumed during the rolling process having its effect on the mechanical properties of the composites. After the processing, the strip was cut in three and the part entering the roll first was designated as Hot-Region (HR) and the rear part, entering the roll, the last was designated as Cold-Region (CR). Normally, with the ARB process, a number of cycles is needed for optimized mechanical properties and ultrafine grained structure. According to Tsuji [39], there is no significant effect until the third cycle in terms of increasing the mechanical properties. Argentero [42] found that in order to improve the mechanical properties, at least 9-13 cycles of repetitive rolling are needed.

3.3.1 Microstructure

AA1070 based composite

Microstructure observation was performed for hot and cold regions of the samples. Influence of compressive deformation on the changes in the grain morphology was analyzed. In the cold region of sample AA1070, peeling and damaged grains can be observed, as shown in Fig. 3.11 (a). Fig 3.11 (b) shows HR in the direction of rolling where welding becomes dominant, resulting in grain growth. ARB process resulted in a reduction in volume and damage to the surface in the form of a deep groove along the shear direction due to the deformation by the delamination mechanism [85-87]. Fig 3.11 (c) shows the delamination in the cold zone. The contact between the matrix and embedded Al_2O_3 nanofibers is blocked by the remaining gas in the micro-pores, so that it results in an incomplete interphase bonding layer. HR in Fig 3.11 (d) shows the grain growth and Al_2O_3 nanofibers effectively embedded into the matrix and reduced porosity. The fracture of Al_2O_3 layer caused the deformation of ARB, followed by the separation of fragments of Al_2O_3 during deformation. Fragmented Al_2O_3 broke down into particles uniformly distributed throughout the aluminum matrix during the cycles of ARB. Comparison with non-aligned nanoparticles was also made. First, 6 wt. % of nanofibers were mixed into aluminum powder by low-energy wet ball milling to misalign the fibers in AA1070 powder. This composite powder was used as reinforcement between the AA1070 strips during ARB. In cold regions, as shown in Fig. 3.11 (e), the delamination distributed in the boundary area occurs. Fig. 3.11 (f) shows hot regions where macro-porosity is reduced by the higher processing temperature. Nevertheless, a significant amount of remaining porosity is still present.

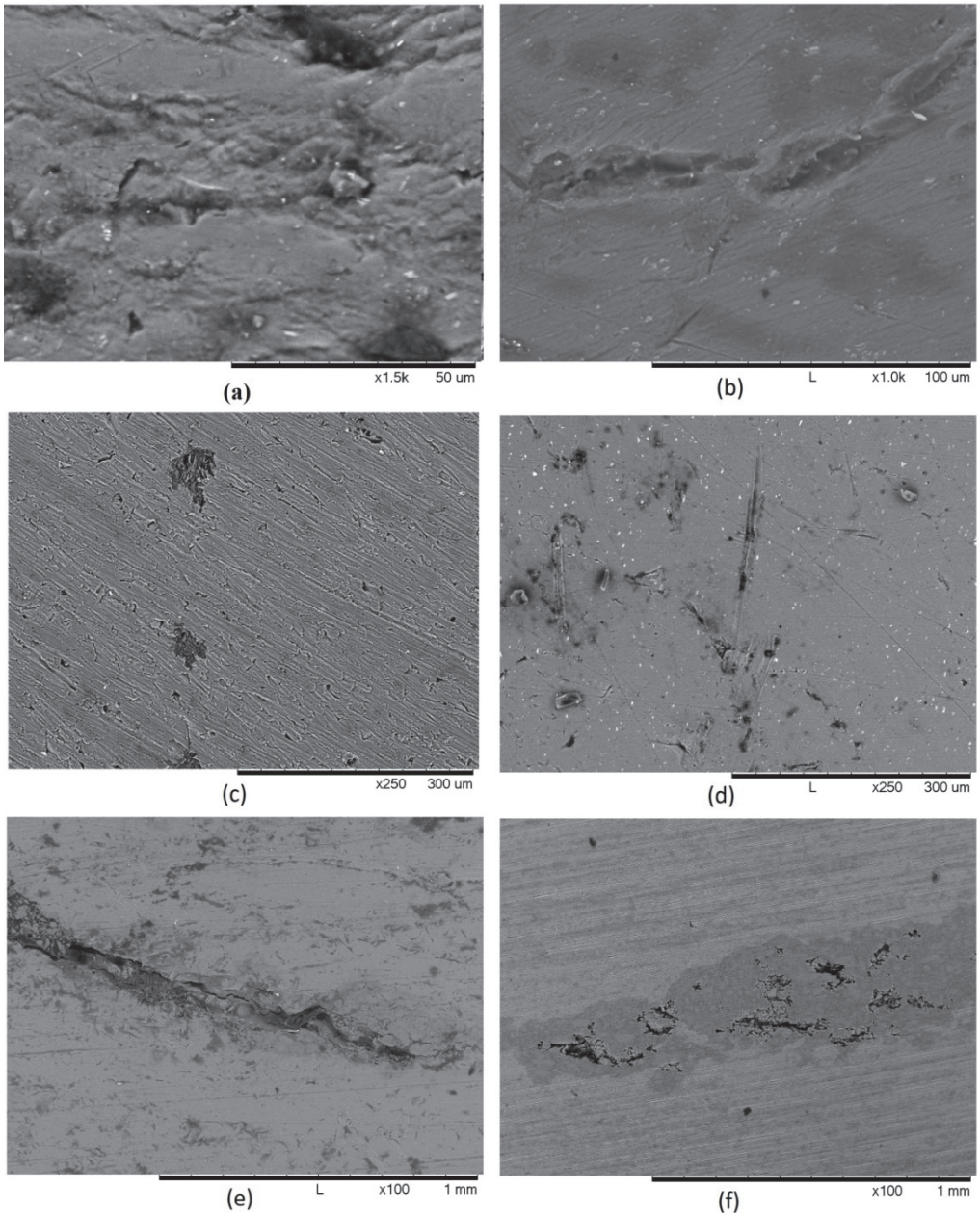


Figure 3.11 Microstructure of AA1070 based composite by the ARB process: (a) pure AA1070-CR; (b) pure AA1070-HR; (c) AA1070 + Al₂O₃ nanofiber-CR; (d) AA1070 + Al₂O₃ nanofiber-HR; (e) AA1070 + AA1060 Powder + Al₂O₃ nanofiber-CR; (f) AA1070 + AA1060 Powder + Al₂O₃ nanofiber-HR.

AA7075 based composite

Microstructure of AA7075 after the ARB process is shown in Fig. 3.12 (a) and (b); with ANF reinforced AA7075 (Fig. 3.12 (c) and (d)). It is evident that the first cycle is not sufficient to immerse ANF into the interphase, as large pores are seen at the contact area among ANF and matrix (Fig. 3.12 (d)).

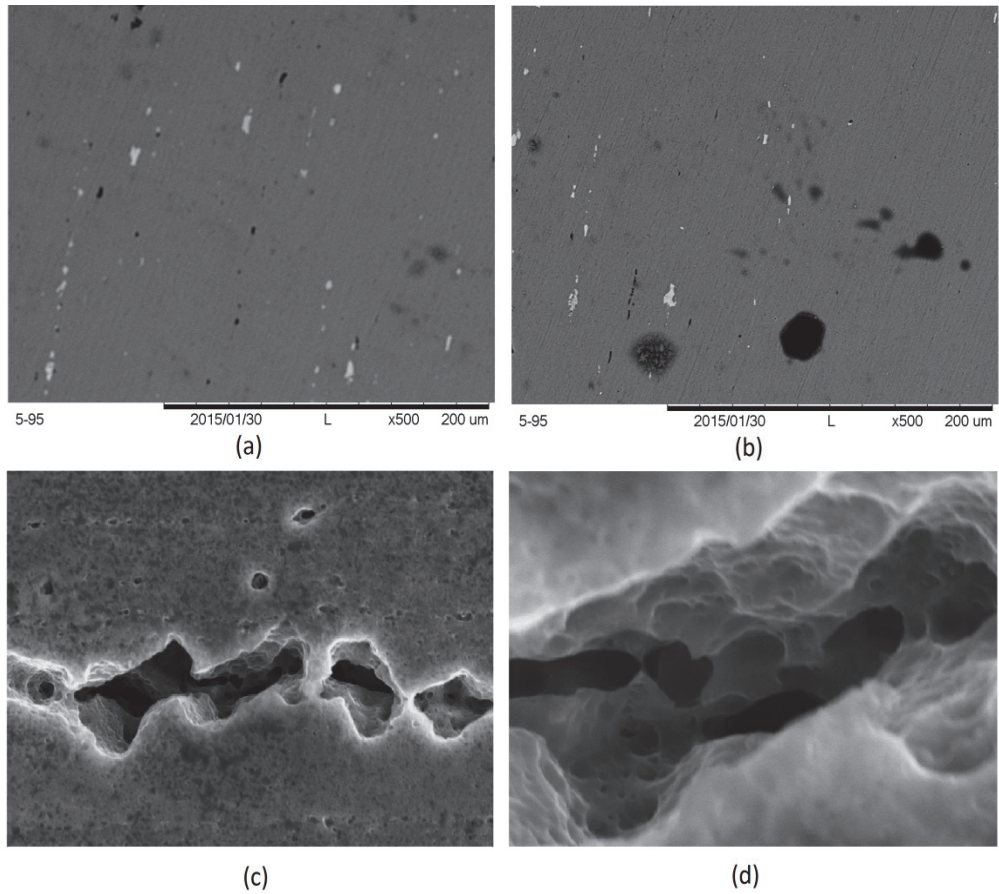


Figure 3.12 Microstructure of AA7075 based composite by the ARB process: (a) AA7075; (b) Dendrite on AA7075; (c) AA7075 + Al₂O₃ nanofiber; (d) macro-porosity on AA7075.

ARB process results in grain growth, on the other hand, consolidation is restrained by Al₂O₃ nanofiber as reinforcement. The recrystallization produced a finer grain structure. Aluminum oxide particles and oxide films formed on the surface and the inclusion spread during roll pressing and acted as a barrier to grain growth.

3.3.2 Mechanical properties

AA1070 based composites

Mechanical properties depend on the temperature applied during ARB cycles. Table 3.3 shows the results of mechanical properties. Hardness of AA1070 in HR was 44 HV10, which is higher than hardness in CR, which was 40 HV10. The higher hardness is accompanied by an increase in density and tensile strength of 148 MPa on HR, as compared to 130 MPa at CR (Fig. 3.13). Increase of hardness and tensile strength during ARB is minimal after the first cycle. Increase of mechanical properties occurs gradually, corresponding to the increase in the number of cycles, optimized at the tenth cycle. For composite AA1070+ANF, higher hardness occurs in CR, which is 48 HV10 compared to HR hardness of 44 HV10. Density does not change significantly. Neither does tensile strength and elongation increase significantly, in HR tensile strength is 144 MPa with 2.7% elongation and CR 113 MPa elongation 2.5%. UFG structure on the ARB process is usually achieved in the eighth cycle's later processes of stable cycles and as a result hardness and tensile strength are increased.

Table 3.3 Mechanical Properties of Al based composite in the ARB process

ARB Process	Hardness HV10	Tensile Strength (MPa)	Elongation (%)	Density (g/cm³)	Grain Size (μm)
AA1070-CR	41±1	130	4	2.74 ±0.02	1.2
AA1070-HR	44±2	148	3.2	2.79 ± 0.31	1.1
AA1070 + ANF-CR	48±1	113	2.5	2.72 ± 0.01	1.9
AA1070 + ANF-HR	45±1	114	2.7	2.73 ± 0.02	1.9
AA1070 + AA1060p + ANF-CR	34±3	57	0.9	2.67± 0.02	6.7
AA1070 + AA1060p + ANF-HR	32±3	96	0.5	2.65 ± 0.03	2.3
AA7075	128±4	-	-	2.81±0.014	1.4
AA7075 + ANF	103±3	-	-	2.79±0.003	1.3

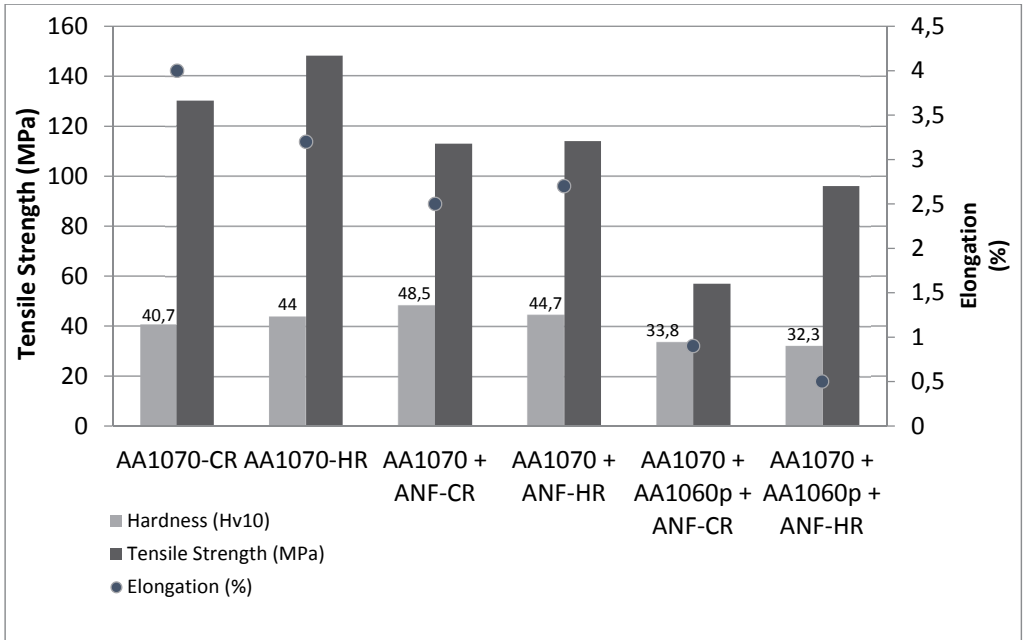


Figure 3.13 Mechanical properties of aluminum based composites.

With the addition of 6 wt. % AA1060 composite powder between AA1070 strips, the mechanical properties were decreased. Hardness of CR was 33 HV10 and 32 HV10 in HR. Density of all of the samples was decreased (2.67g/cm^3 in CR and 2.65g/cm^3 in HR). The tensile strength in CR 57 MPa was lower than that in HR, which was 96 MPa. As shown in Fig. 3.13, although tensile strength had higher HR, elongation was lower. In CR, micro-porosity was gathered in the area of delamination, while in HR; micro-porosity was gathered in the interphase region, so that heat on ARB reduces micro-porosity at the interface.

AA7075 based composites

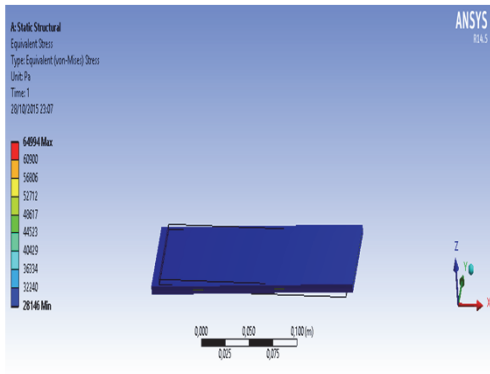
The hardness of AA7075 in CR is 128 HV10 with density corresponding to theoretical density (2.8g/cm^3). The ANF reinforcement in AA7075 based composite decreases the hardness to 103 HV10, accompanied by the decrease in density. The decrease in hardness is due to porosity at the interphase among AA7075 as matrix and ANF (in Fig 3.12 (c-d)). This results in a weak bond between the matrix and reinforcement. Saito [10] recommended to increase the number of optimum cycles in order to achieve a strong bonding. The ARB processes on the thirteenth cycle in the composite showed the presence of large particles and the structure of deformation around the particles, strengthening the particles in the matrix and also eliminating porosity in the interface of a Al/Al₂O₃ based composite. The mechanical properties of the AA7075 based composite are confirmed in Table 3.3.

3.3.3 Determination of the parameters of the ARB process using the FEM analysis

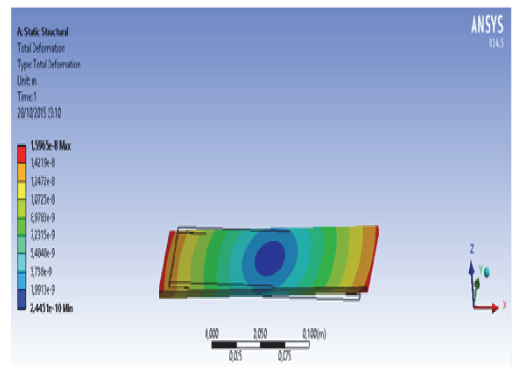
The pressure and temperature on ARB is important in the process to determine the viability to improve the material properties of composites. FEM helps to solve various technical problems associated with process parameters on ARB. Govindaraj [88] used FEM to simulate deformation, instability combination of different material by ARB. Mode instability observed with dimensions of FEM simulation was conducted, in which the direction movement of pressure was forming 45° type of sinusoidal bending of the strongest layer by shear bands. Stronger layers occur when the alloy was elongated, thus work hardening the metal layer. FEM analysis was also used by Lihong [89] for the optimization of surface roughness on AA1050/AA6061. At the fifth cycle of ARB, the resulted surface roughness can generate good bonding without lubrication.

Pressure distribution analysis

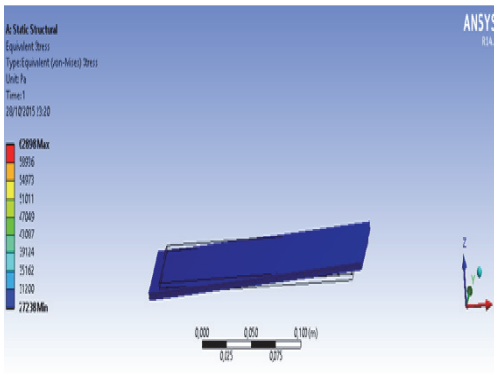
The first cycle of high pressure of rolling spreading on the surface of aluminum plate is shown in Fig. 3.14 (a-b) for the first cycle of ARB. It was observed that ANF is cut by tensile rolling load, confirmed in Fig. 3.14 (e). ANF has a length of 50 mm, 1 mm thick, and weighing 0.6 g, placed between the aluminum plates. In the second cycle, the pressure of rolling tends to further decrease stress distribution, as can be seen in Fig. 3.14 (c-d). On the second cycle of load rolling, the embedded Al_2O_3 nanofiber was well-adhered to the surface of the aluminum plate, as shown in Fig. 3.14 (f).



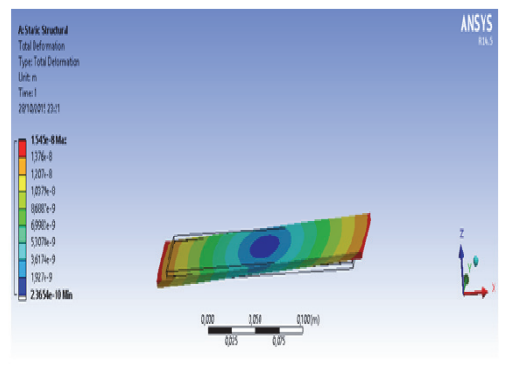
(a)



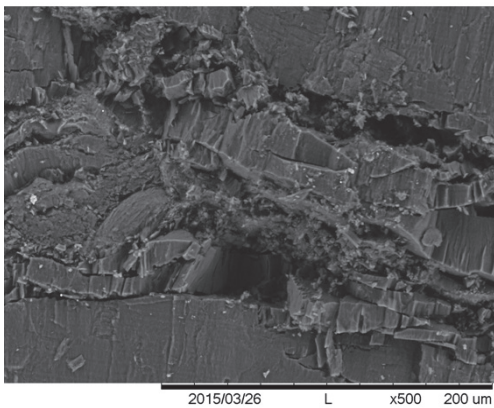
(b)



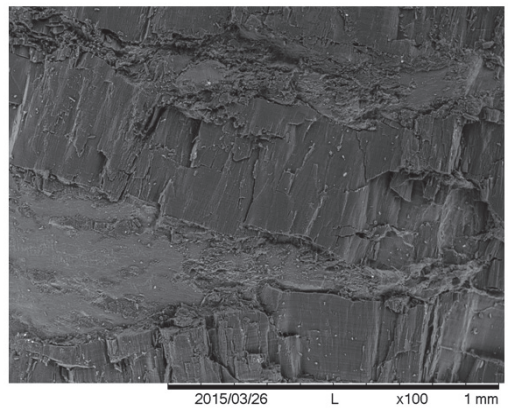
(c)



(d)



(e)



(f)

Figure 3.14 FEM analysis of stress-strain distribution of the ARB process: (a) stress on the first cycle; (b) strain on the first cycle; (c) stress on the second cycle; (d) strain on the second cycle; (e) ANF disconnected during the first cycle (f) ANF embedded during the second cycle.

The deformation of the ARB process is capable of producing strain that is not limited because the number of cycles of ARB can be repeated unlimitedly (indefinitely). The consideration of a practical factor, such as strain hardening, normal pressure of compression requirements, and edge cracking, limits the maximum number of ARB cycles applicable. A reduction of 50% usually applied in each cycle of ARB with the type of reduction strip thickness (t) after cycle (n) is shown in the following equation:

$$t = \frac{t_0}{2^n} \quad (3.1)$$

where t_0 is initial thickness on the strips, after (n) cycles, total reduction r_t is given by:

$$r_t = 1 - \frac{t}{t_0} = 1 - \frac{1}{2^n} \quad (3.2)$$

The equation of plastic strain ε assumed by the theory of Von Misses yield criteria, plane strain condition is given by

$$\varepsilon = \left(\frac{2}{\sqrt{3}} \ln \left(\frac{1}{2} \right) \right) n = 0.8n \quad (3.3)$$

The ARB process is capable of reducing a ± 1 mm thick sheet to approximately $1 \mu\text{m}$ after 10 cycles. An example to change the geometry when two 1 mm thick sheets are rolled bonded with a 50% deformation in each ARB cycle is provided in Table 3.4. When the process of ARB on Al/Al₂O₃ nanofiber composite is repeated for the second time, the initial thickness is reduced to $\frac{1}{4}$. When 2.5 mm of thickness is reduced to 1 mm, the achieved total reduction is 75% and the total equivalent plastic strain is 1.6. This process can introduce ultra-high strain into a composite material by ARB.

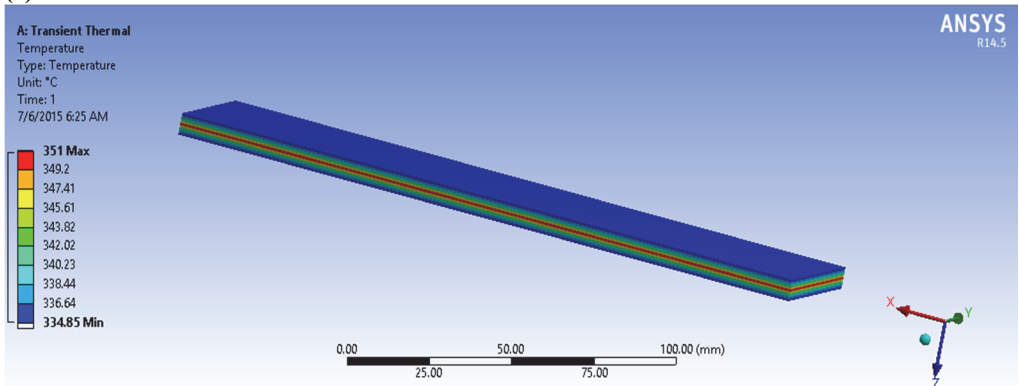
Table 3.4 Changes of materials geometry during ARB on two 1mm sheets by 50% reduction per cycle

No of cycles	1	2	3	4	5	6	7	8	9	10	n
No of layers	2	4	8	16	32	64	128	256	512	1024	2^n
No of bonded boundaries	1	3	7	15	31	63	127	255	511	1023	$2^n - 1$
Layer interval (μm)	500	250	125	62.5	31.2	15.6	7.8	3.9	1.9	0.96	$1000/2^n$
Total reduction (%)	50	75	87.5	93.8	96.9	98.4	99.2	99.6	99.8	99.9	$(1 - 1/2^n) \times 100$
Equivalent strain	0.8	1.6	2.4	3.2	4.0	4.8	5.6	6.4	7.2	8.0	$\left(\frac{2}{\sqrt{3}} \ln 2 \right) n = 0.8n$

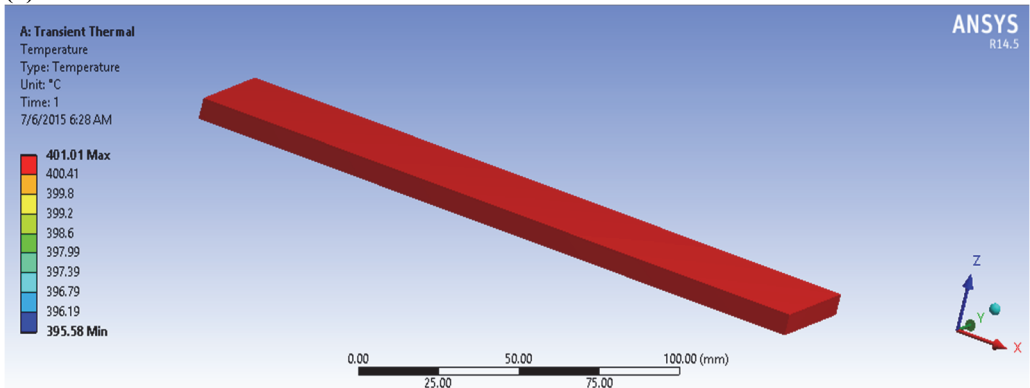
Temperature distribution analysis

Rolling process at an increased temperature induces recrystallization, therefore, it is expected to get high formability process and avoid defects in the product. In the process of ARB, AA1070/AA7075 composite has the upper recrystallization temperatures at 400-500 °C. Fig. 3.15 (b-c) shows FEM simulation where red color represents the entire surface indicating the excessive temperature, thereby some parts possess dendrite formation (Fig. 3.15 (e-f)). The temperature affects the grain size and arrangement of grain boundaries in the microstructure, a temperature upper limit between 400-500 °C causes dynamic recrystallization, resulting in the nucleation of new grains that become dendrites. The use of temperature between 300-399 °C (Fig. 3.15 (a)) resulted in grain distribution without dendrites, confirmed in Fig. 3.15 (d). ARB process should be conducted at elevated temperatures below recrystallization temperature because then it cancels out the accumulated strains; a low temperature would result in insufficient ductility and bond strength, where material can be bonded together despite no recrystallization.

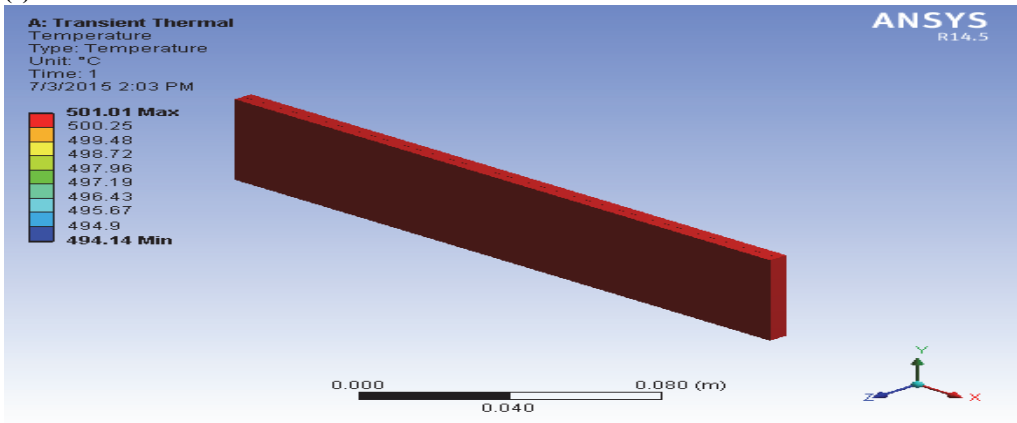
(a)



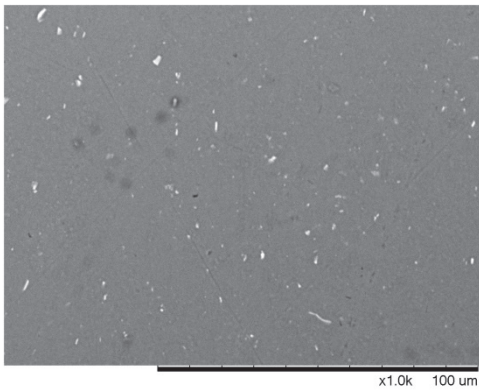
(b)



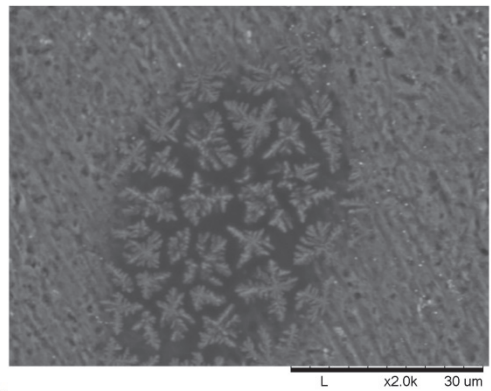
(c)



(d)



(e)



(f)

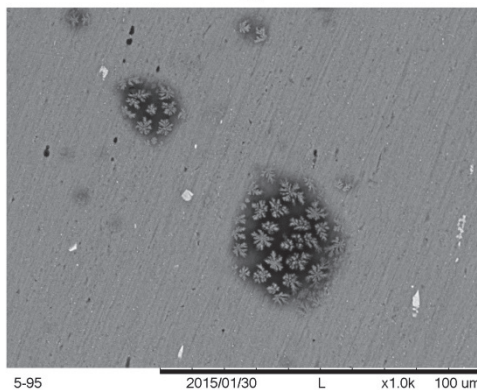


Figure 3.15 FEM analysis of temperature distribution: (a) preheated to 350 °C; (b) preheated to 400 °C; (c) preheated to 500 °C; (d) grain distribution at 350 °C; (e) dendrite at 400 °C; (f) dendrite at 500 °C.

3.3.4 Microstructure evolution of Al based composite after the second cycle of ARB

Based on the description of the theory and results from ARB experiments, Al based composite can be explained by the phenomenon of microstructural evolution. During the first cycle, ANF was truncated by compression from the roll contact. During the second cycle, ANF was embedded on the stack of aluminum as matrix. The use of higher temperature helps to provide bonding between the matrix and reinforcement, as explained in Fig. 3.16. Selection of the temperature is very important for increasing formability, but at a certain temperature (400–500 °C), dendrite formation inhibits nanofiber reinforcement.

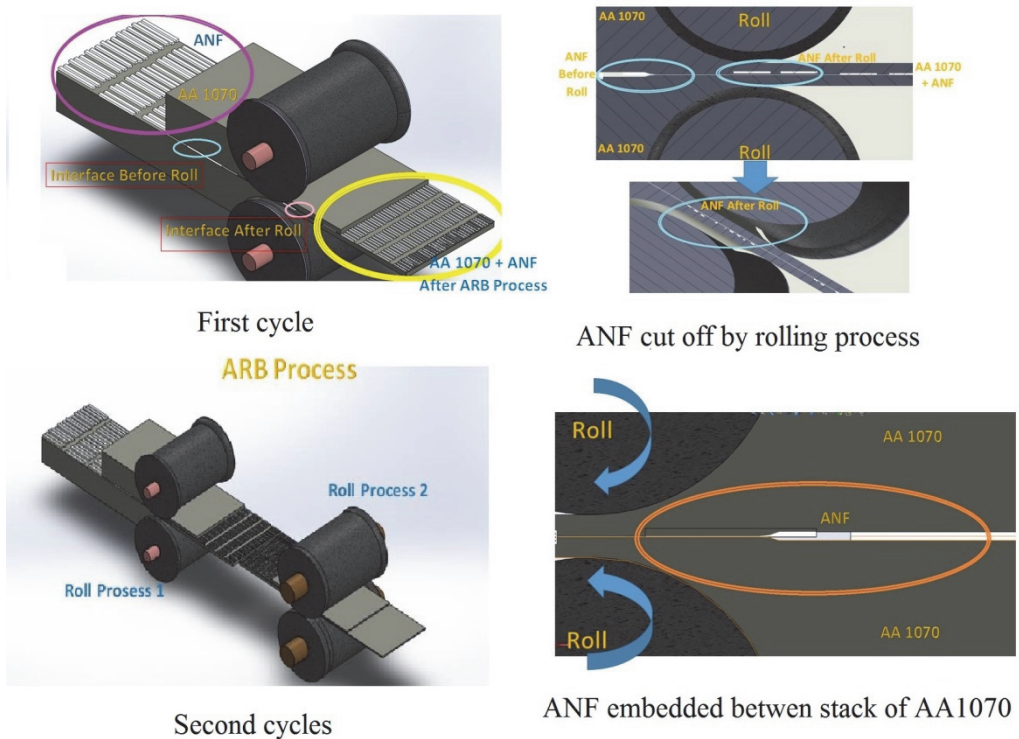


Figure 3.16 Modeling of formation of bonding mechanism between Al/ANF ARB processes.

To produce an ultrafine grained structure, a large number of cycles ARB is needed. Argentero [42] performed 10 cycles of ARB, while Jamaati [90] reached eight cycles to generate significant mechanical properties. A large number of cycles in general is unacceptable for mass production in the industry.

3.4 Aluminum based composites by RPRB

3.4.1 Microstructure

Repetitive Press Roll Bonding (RPRB) is a new method of SPD that is expected to be able to reduce the number of cycles needed for the ARB process: to obtain sufficient bonding with grain refinement. The end result is an alloy with thorough bonding of matrix and reinforcement, as seen in Fig. 3.17 (a). The first pass of uniaxial pressing distributes Al₂O₃ nanofiber at the interphase (Fig. 3.17 (b)) and some macro-porosity is remained, as seen in Fig. 3.17 (d). Al₂O₃ nanofiber partially unattached from the interphase was also seen. After the first cycle (Fig. 3.17 (e)), RPRB showed embedding of Al₂O₃ nanofibers and sufficient bonding as there is no micro-porosity found at the interphase (Fig. 3.17 (f)).

3.4.2 Mechanical properties

Hardness

The hardness of AA1070 by uniaxial pressing process is 38 HV10, hardness increases with addition of Al₂O₃ nanofiber up to 42 HV10. The hardness value compares to that produced by RPRB of AA1070, which is at 42 HV10, accompanied by decreased density of 2.6 g/cm³. After the addition of Al₂O₃ nanofiber, hardness increases slightly to 44 HV10. This increase occurred on the first cycle 48 HV10, which is almost equal to the hardness of the ARB on CR. During the second cycle, the hardness increases significantly up to 53 HV10. The mechanical properties are presented in Table 3.5.

Table 3.5 Mechanical properties of RPRB alloys

Materials	Hardness HV10	Density (g/cm ³)	Tensile Strength (MPa)	Elongation (%)	Grain Size (μm)
AA1070 by uniaxial pressing	38±5	2.7±0.02	139	0.4	2.0
Al based composite by uniaxial pressing	42±2	2.6±0.04	91	0.1	3.0
AA1070 by RPRB	42±4	2.6+0.05	157	2.8	2.2
Composite by RPRB	44±6	2.6±0.05	163	1.3	3.0
RPRB On first cycles	48±1	2.7±0.10	170	4	2.1
RPRB On second cycles	53±2	2.7±0.09	290	9	1.5

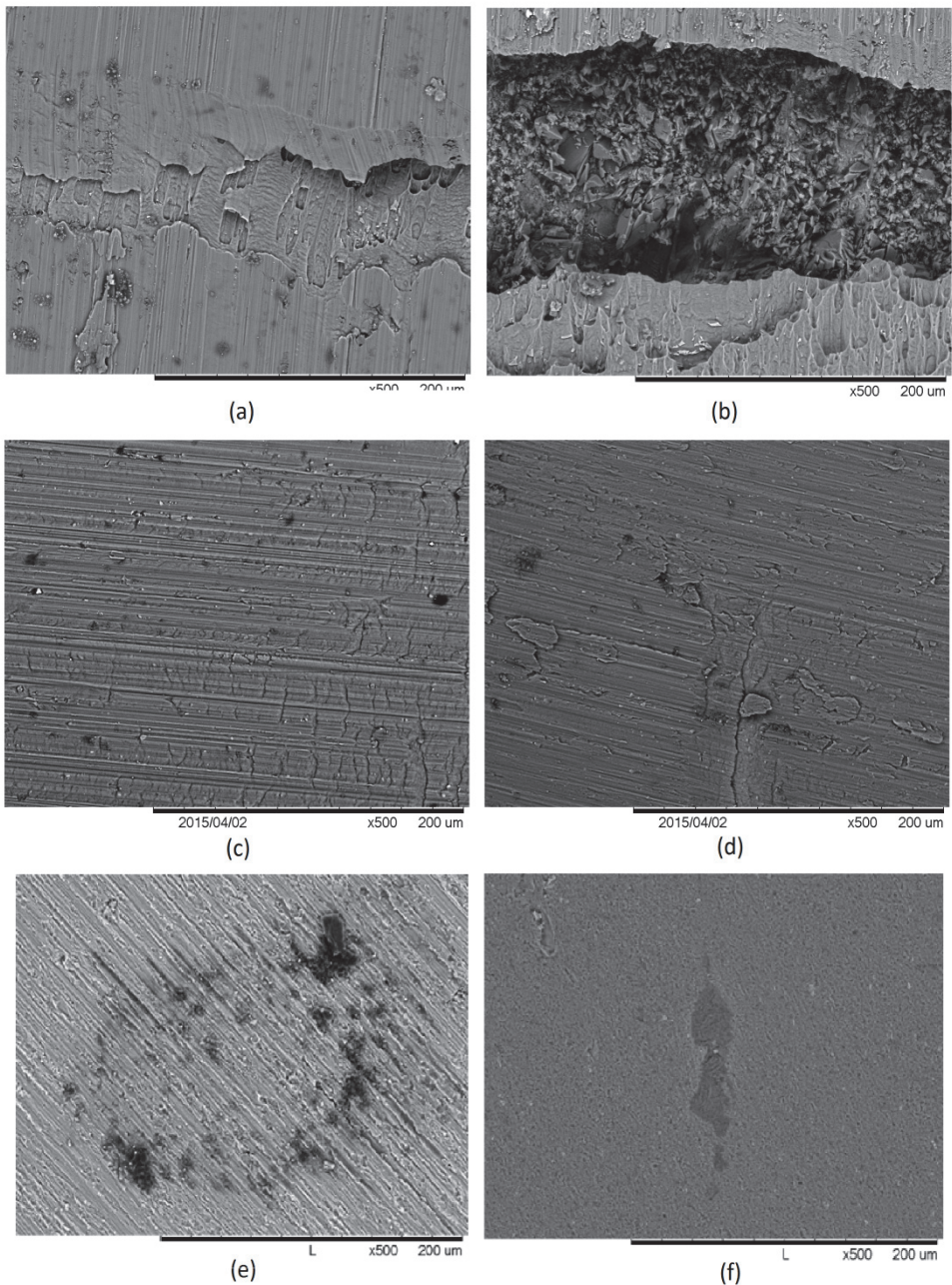


Figure 3.17 Microstructure of Al based composite: (a) AA1070 by uniaxial pressing process; (b) AA1070+ANF by uniaxial pressing process; (c) AA1070 by RPRB process; (d) AA1070+ANF by RPRB process; (e) Al based composite after first cycle of RPRB; (f) Al based composite after second cycles of RPRB.

Tensile strength

The tensile strength of AA1070 by uniaxial pressing before the rolling process was 139 MPa with elongation of 0.4%. After the addition of Al₂O₃ nanofibers reinforcement, the tensile strength was decreased to 91 MPa with elongation of 0.1%. The decrease was caused by Al₂O₃ to be a barrier at the interphase bonding between aluminum as matrix and Al₂O₃ nanofiber as reinforcement. In the process of RPRB, the tensile strength of AA1070 was increased, after adding of Al₂O₃ nanofiber, the tensile strength increased from 157 MPa to 163 MPa, but the elongation decreased from 2.8% to 1.3%, an increase in the tensile strength was due to the additional effect of reinforcement. However, there was a decline in the elongation caused by imperfect bonding between the interphases. During the second cycle, there was a drastic increase in the tensile strength of 170 MPa to 290 Mpa, accompanied by an increase in elongation from 4% to 9%; the result of tensile strength is confirmed in Fig. 3.18.

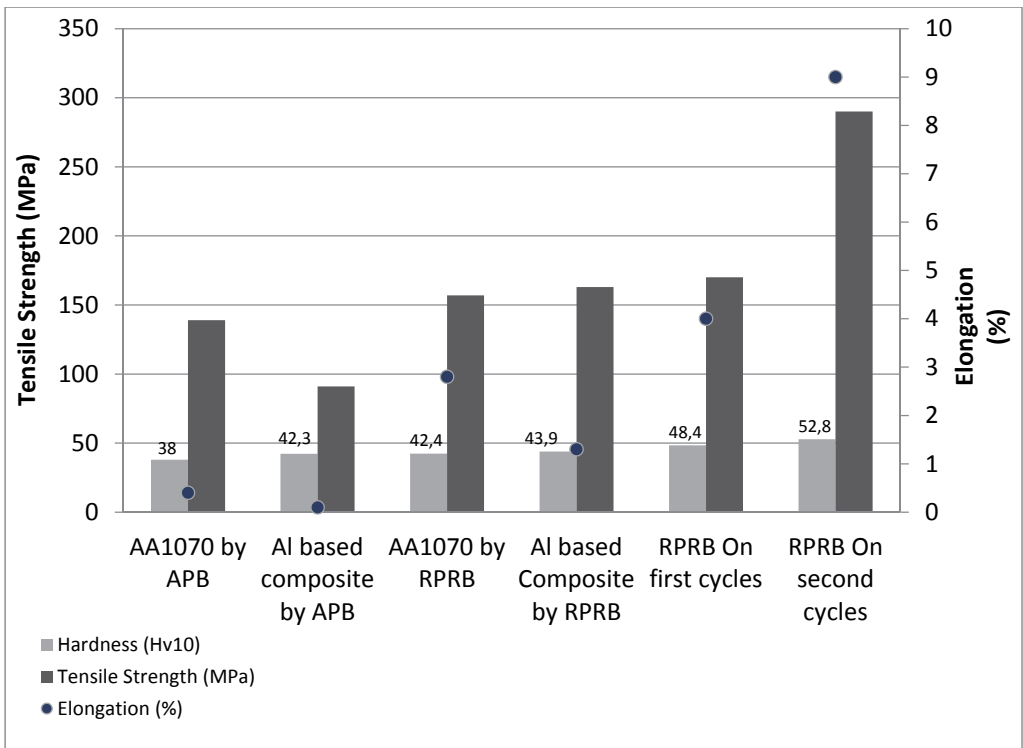
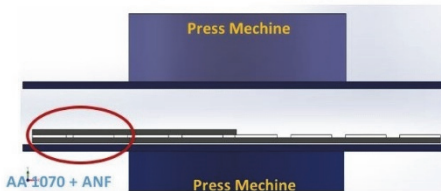


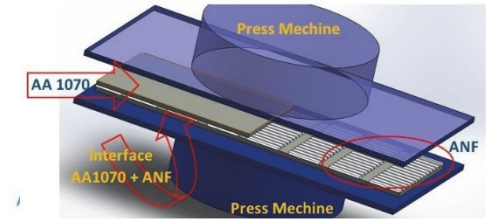
Figure 3.18 Tensile strength of AA1070 based composite by the RPRB process.

3.4.3 Evolution of microstructure in the RPRB process

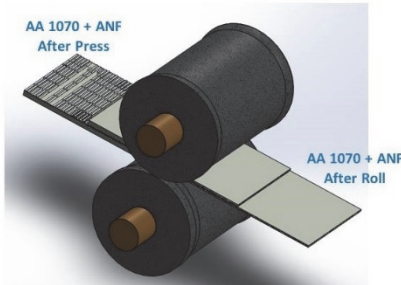
The first cycles of the RPRB process is capable of cutting and immersing ANF simultaneously within a stack of aluminum, whereas in the ARB process, this should be done in two cycles. In the second cycle, in the rolling process, the grain size becomes finer. This makes it possible to form an interface bonding between the aluminum matrix and ANF as reinforcement. This is evidenced by a significant increase in mechanical properties in the results of the aluminum-based composite RPRB process after the second cycles.



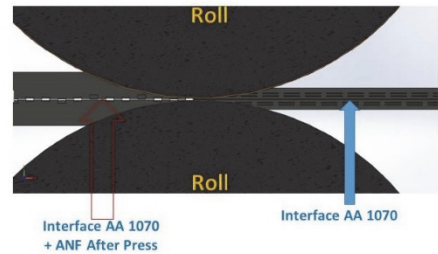
Uniaxial pressing



ANF cut off and embedded simultaneously by pressing process



Roll bonding



ANF distributed evenly and produced a fine grain and form a interface bonding

Figure 3.19 Bonding mechanism between Aluminum and Al_2O_3 nanofibers during RPRB process.

CONCLUSIONS

The results of the development of SPD technologies for consolidation of aluminum alloy powders show that ultrafine grained bulk alloys with acceptable strength and ductility can be obtained with alloys 6061 and 7075. Heat treatment has a dual effect of grain coarsening and formation of precipitates. For alloys with low formability, e.g. 7075, solution heat treatment and artificial aging as post heat treatment is recommended.

Equal parallel channel angular pressing was shown to be a viable route to produce Al/Al₂O₃ nanofiber composites. Due to more uniform strains during the processing, integrity of the parts was obtained even after a higher number of passes. It takes up to four cycles to produce composites with ultrafine grained structure

Accumulative Roll Bonding process, as one of the few technologies available, allows production of metal matrix composites with aligned nanofibers. It was shown that during the ARB process, the Al₂O₃ nanofibers are cut due to the tensile stresses applied during rolling. Starting from the second cycles, Al₂O₃ nanofibers start to be embedded in the matrix. Clear evidence of the positive effect of aligned versus non-aligned nanofibers was shown when considering strength and elongation of the composites. An important processing parameter was found to be the temperature of compaction; even small deviations below the crystallization temperature produce dendrites that cancel high strains; therefore they have a higher number of defects in composites.

A novel technology called repetitive press rolls bonding was developed, which combines pressing and rolling. The new technology simplifies the ARB process, and eases the embedding of reinforcement like Al₂O₃ nanofibers. Processing time is reduced, for instance, to embed Al₂O₃ nanofibers, only one cycle is needed and the result is a strong bonding.

The scientific novelty of research

- For the first time, aligned ceramic nanofibers were embedded effectively in aluminum alloy matrices. The nanocomposites were fabricated using accumulative roll bonding process. The bundles of starting nanofibers, having a length of ~13 cm and a diameter of 7 nm, were embedded in the aluminum matrix already after two passes. Although the nanofiber was shortened during the process, distinct benefits regarding mechanical properties were obtained, when compared with nanocomposites with non-aligned nanofibers.

- Importance of temperature fluctuations during processing of aluminum based nanocomposites was revealed. During equal parallel channel angular pressing, high temperatures are needed for effective compaction. During ARB, even cooling of the strip during the cycle has a significant impact on the mechanical properties and microstructure.

REFERENCES

1. Haghghi, R.D.; Jahromi, S.A.J.; Moresedgh, A.; Khorshid, M.T., Comparison between ECAP and conventional extrusion for consolidation of aluminum metal matrix composite. *ASM International, Journal of Materials Engineering and Performance*, 2012, 21 (9), 1885-1892.
2. Callister, W. D., Introduction material science and engineering, John Wiley & Sons, Inc, 1999, Fifth edition.
3. ASM Metals Handbook, Properties and selection nonferrous alloys and special purpose materials, Vol. 2, ASM International, 1992.
4. Xia, K.; Wu, X., Back pressure equal channel angular consolidation of pure Al particles, *Scripta Materialia*, 2005, 53 (11), 1225-1229.
5. Matsuki, K.; Aida, T.; Takeuchi, T.; Kusui, J.; Yokoe, K., Microstructural characteristics and superplastic-like behavior in aluminum powder alloy consolidated by equal channel angular pressing, *Acta Materialia*, 2000, 48 (10), 2625-2632.
6. Senkov, O.N.; Miracle, D.B.; Scott, J.M.; Senkova, S.V., Equal channel angular extrusion compaction of semi-amorphous $Al_{85}Ni_{10}Y_{2.5}La_{2.5}$ alloy powder, *Journal of Alloys and Compounds*, 2004, 365 (1), 126-133.
7. Robertson, J.; Im, J.T.; Karaman, I.; Hartwig, K.T.; Anderson, I.E., Consolidation of amorphous copper based powder by equal channel angular extrusion, *Journal of Non-Crystalline Solids*, 2003, 317 (1-2), 144-151.
8. Valiev, R.Z.; Langdon, T.G., Achieving exceptional grain refinement through severe plastic deformation: new approaches for improving the processing technology, *Metallurgical and Materials Transactions A*, 2011, 42 (10), 2942-2951.
9. Murashkin, M. Y.; Bobruk, E.V.; Kil'mametov, A.R.; Valiev, R.Z., Structure and mechanical properties of aluminum alloy 6061 subjected to equal-channel angular pressing in parallel channels. *The Physics of Metals and Metallography*, 2009, 108 (4), 415-423.
10. Saito, Y.; Utsunomiya, H.; Tsuji, N.; Sakai, T., Novel ultra-high straining process for bulk materials development of the accumulative roll-bonding (ARB) process. *Acta Materialia*, 1999, 47 (2), 579-583.
11. Chang, S.Y.; Lee, K.S.; Ryu, S.K.; Park, K.T.; Shin, D.H., Effect of equal channel angular pressing on the distribution of reinforcements in the discontinuous metal matrix composites. *Materials Transactions*, 2002, 43 (4), 757-761.
12. Ramesh, D.; Swamy, R.P.; Chandrashekar, T.K., Role of heat treatment on Al6061- frit particulate composites. *Journal of Minerals & Materials Characterization & Engineering*, 2012, 11 (4), 453-462.

13. Fukuda, Y.; Oh-ishi, K.; Furukawa, M.; Horita, Z.; Langdon, T.G., The application of equal-channel angular pressing to an aluminum single crystal, *Acta Materialia*, 2004, 52 (6), 1387-1395.
14. Valder, J.; Rijesh, M.; Surendranathan, A.O., Forming of tubular commercial purity aluminum by ECAP. *Materials and Manufacturing Processes*, 2012, 27 (9), 986–989.
15. Azushima, A.; Kopp, R.; Korhonen, A.; Yang, D.Y.; Micari, F.; Lahoti, G.D.; Groche, P.; Yanagimoto, J.; Tsuji, N.; Rosochowski, A.; Yanagida, A., Severe plastic deformation (SPD) processes for metals, *CIRP Annals - Manufacturing Technology*, 2008, 57 (2), 716-735.
16. Valiev RZ, Nanostructured of metals by severe plastic deformation for advanced properties. *Nature materials*, 2004, 3 (8), 511-516.
17. Wu, X.; Xia, K., Back pressure equal channel angular consolidation application in producing aluminum matrix composites with fine flyash particles, *Journal of Materials Processing Technology*, 2007, 192 (193), 355-359.
18. Murashkin, M. Y.; Sabirov, I.; Kazykhanov, V.U.; Bobruk, E.V.; Dubravina, A. A.; Valiev, R. Z., Enhanced mechanical properties and electrical conductivity in ultrafine-grained Al alloys processed via ECAP-PC, *Journal of Materials Science*, 2013, 48 (13), 4501-4509. .
19. Umemoto, M., Nanocrystallization of steels by severe plastic deformation, *Materials Transaction*, 2003, 44 (10), 1900-1911
20. Segal, V.M.; Korbel, A.; Richert, M.; Richert, J., in: Second RISO International Symposium on Metallurgical Science, *Material Science Engineering*, 1999, A271, 322.
21. Segal, V.M., Severe plastic deformation: simple shear versus pure shear, *Materials Science and Engineering*, 2002, A338, 331-334.
22. Valiev, R. Z.; Korznikov, A.V.; Mulyukov, R. R., Structure and properties of ultrafine-grained materials produced by severe plastic deformation, *Materials Science and Engineering*, 1993, A168 (2), 141-148.
23. Valiev, R. Z.; Islamgaliev, R. K.; Alexandrov, I. V., Bulk nanostructured materials from severe plastic deformation, *Progress in Materials Science*, 2000, 45 (2), 103-189.
24. Valiev, R. Z.; Langdon, T. G., Principles of equal channel angular pressing as a processing tool for grain refinement, *Progress in materials Science*, 2006, 51, 881-981.
25. Han, B. Q.; Matejczyk, D.; Zhou, F.; Zhang, Z.; Bampton, C.; Lavernia, E. J. Mechanical behavior of a cryomilled nanostructured Al-7.5 pct mg alloy, *Metallurgical and Materials Transactions A*, 2004, 35A, 947-950.
26. Langdon, T. G.; Furukawa, M.; Nemoto, M.; Horita, Z., Using equal-channel angular pressing for refining grain size, Nanoscale Materials Overview, *Journal of The Minerals, Metals & Materials Society*, 2000, 30-32.

27. Langdon, T. G., The principles of grain refinement in equal-channel angular pressing. *Materials Science and Engineering*, 2007, A462 (1), 3–11.
28. Furukawa, M.; Horita, Z.; Nemoto, M.; Langdon, T. G., Review: processing of metals by equal channel angular pressing, *Journal of Material Science*, 2001, 36 (12), 2835-2843.
29. Comwall, L. R.; Hartwig, K. T.; Goforth, R. E.; Semiatin, S.L., The equal channel angular extrusion process for materials processing, *Materials Characterization*, 1996, 37 (5), 295-300.
30. Valiev, R. Z.; Langdon, T. G., Development in the use of ECAP processing for grains refinement. *Reviews on Advanced Material Science*, 2006, 13, 15-26.
31. Xue, Q.; Beyerlein, I. J.; Alexander, D. J.; Gray, G. T., Mechanisms for initial grain refinement in OFHC copper during equal channel angular pressing. *Acta Materialia*, 2007, 55, 655-668.
32. Huang, X.; Wang, K.; Wu, S. D.; Zhang, Z. F.; Li, G. Y.; Li, S. X., Deformation twinning in polycrystalline copper at room temperature and low strain rate, *Acta Materialia*, 2006, 54, 655-665.
33. Valiev, R. Z., Recent developments of severe plastic deformation techniques for processing bulk nanostructured materials, *Materials Science Forum*, 2008, 579, 1-14.
34. Valiev, R. Z.; Murashkin, M. Y.; Bobruk, E. V.; Raab, G. I., Grain refinement and mechanical behavior of the Al alloy, subjected to the new SPD technique, *Materials Transactions*, 2009, 50 (1), 87-91.
35. Djavanroodi, F.; Ebrahimi, M., Effect of die parameters and material properties in ECAP with parallel channels. *Materials Science and Engineering A*, 2010, 527 (29), 7593-7599.
36. Mihhalsenkov, M., Production elaboration and characterization of Al/B₄C based composite, Department Materials Engineering, Tallinn University of Technology, MsC Thesis, 2012, 21-25.
37. Liu, Z. Y.; Liang, G. X.; Wang, E. D.; Wang, Z. R., *Materials Science and Engineering*, 1998, A242, 137-140.
38. Kim, W. J.; Kim, J. K.; Park, T. Y.; Hong, S. I.; Kim, D. I.; Kim, J. S.; Lee, J. D., Enhancement of strength and superplasticity in a 6061 Al alloy processed by equal channel angular pressing, *Metallurgical and Materials Transactions A*, 2002, 33 (10), 3155-3164.
39. Tsuji, N.; Saito, Y.; Lee, S. H.; Minamino Y., Accumulative roll bonding and other new technique to produce bulk ultrafine grained materials, *Advanced Engineering Material*, 2003, 5 (5), 338-344.
40. Tsuji, N.; Shiotsuki, K.; Saito, Y., Superplasticity of ultra-fine grained Al-Mg alloy produced by accumulative roll-bonding, *Materials Transactions*, 1999, 40 (8), 765-771.

41. Tsuji, N.; Saito, Y.; Utsunomiya, H.; Tanigawa, S., Ultra-fine grained bulk steel produced by accumulative roll-bonding (ARB) process, *Scripta Materialia*, 1999, 40 (7), 795-800.
42. Argentero, S., Accumulative roll bonding technology of aluminum alloys, *Proceedings of Strategic Management Factors of MNC's Subsidiaries–Comparative Analysis of Metal Manufacturing and Other Industries in the Czech Republic*, 2012, 1-6.
43. Kuhlmann, D.; Wilsdorf., Properties and effects of low energy dislocation structures. *Materials Science and Engineering*, 1987, 86, 53-66.
44. Bordeaux, F.; Yavari, R., Multiple necking and deformation behaviour of multilayer composites prepared by cold rolling, *Material: Z Metallkunde*, 1990, 81 (2), 130-135.
45. Saito, Y.; Tsuji, N.; Utsunomiya, H.; Sakai, T.; Hong, R.G. Ultra-fine grained bulk aluminum produced by accumulative roll bonding (ARB) process. *Scripta Materialia*, 1998, 39 (9), 1221-1227.
46. Cherukuri, B.; Nedkova, T. S.; Srinivasan, R., A comparison of the properties of SPD-processed AA-6061 by equal-channel angular pressing, multi-axial compressions/forgings and accumulative roll bonding, *Materials Science and Engineering A*, 2005, 410 (411), 394-397.
47. Kozumia, Y.; Ueyama, M.; Tsuji, N.; Minamino, Y.; Ota, K., High damping capacity of ultrafine grained aluminum produced by accumulative roll-bonding (ARB), *Journal of Alloys and Compounds*, 2003, 355 (1), 47-51.
48. Bay N., Cold welding: Part I, Characteristic, bonding mechanisms, bond strength, *Metals Constructions*, 18 (6) (1986), pp. 369–372
49. Inoue, T., Strain variations on rolling condition in accumulative roll-bonding by finite element analysis, *National Institute for Materials Science, Japan In-Tech Europe*, 2010, 590-610.
50. Jamaati, R.; Toroghinejad, M. R.; Edris, H.; Salmani, M. R., Fabrication of nano/ultra-fine grained IF steel via SPD Processes: a review. *Transactions of The Indian Institute of Metals*, 2014, 67 (6), 787-802.
51. Backofen, W. A., *Deformation Processing*, Addison-Wesley Publishing Company., Massachusetts, 1972, 94-115.
52. Dieter, G.E., McGraw-Hill, *Mechanical Metallurgy SI Metric Edition*, 1988, 501-563.
53. Govindaraj, N. V.; Frydendahl, J. G.; Holmedal, B., Layer continuity in accumulative roll bonding of dissimilar materials combinations. *Materials and Design*, 2013, 52, 905-915.
54. Huh, M. Y.; Lee, J. P.; Lee, J. C.; Park, J. W.; Chung, Y. H., Formation of shear texture and ultra-fine grains during equal angular channel rolling and subsequent annealing in AA3003 sheet. *Materials Science Forum*, 2004, 449 (452), 873-876.

55. Miran, S., Severe plastic deformation methods to achieve nanostructured materials, *International Journal of Material Science*, 2014, 4 (3), 99-104.
56. Li, P.; Xue, K. M.; Wang, X.; Qian, C. H., Refinement and consolidation of pure Al particles by equal channel angular pressing and torsion, *Transactions of Nonferrous Metals Society of China*, 2014, 24, 1289-1294.
57. Amirkhanlou, S.; Ketabchi, M.; Parvin, N.; Khorsand, S.; Bahrami, R., Accumulative press bonding a novel manufacturing process of nanostructured metal matrix composites, *Materials and Design*, 2013, 51, 367-374.
58. Shen, Y. F.; Guan, R. G.; Zhao, Z. Y.; Misra, R. D. K., Ultrafine-grained Al–0.2Sc–0.1Zr alloy: The mechanistic contribution of nano-sized precipitates on grain refinement during the novel process of accumulative continuous extrusion. *Acta Materialia*, 2015, 100, 247-255
59. ASM Handbook, *Heat Treating*, ASM International, 1991, 4.
60. Troeger, L. P.; Starke, E. A., Microstructural and mechanical characterization of a superplastic 6xxx aluminum alloy, *Materials Science and Engineering A*, 2000, 277 (1-2), 102-113.
61. Linardia, E.; Haddad, R.; Lanzani, L., Stability analysis of the Mg₂Si phase in AA6061 aluminum alloy, *Procedia Materials Science*, 2012, 1, 550-557.
62. Kumar, P. V.; Reddy, G. M.; Rao, K. S., Microstructure, mechanical and corrosion behavior of high strength AA7075 aluminum alloy friction stir welds e effect of post weld heat treatment. *Defence Technology*, 2015, 11, 362-369.
63. Jiménez, C. M. C.; Infanta, J. M. G.; Ruano, O. A.; Carreno, F., High strain rate superplasticity at intermediate temperatures of the Al7075 alloy severely processed by equal channel angular pressing, *Journal of Alloys and Compounds*, 2011, 509, 9589-9597.
64. NATO science series II, Mathematic, Physics and Chemistry. Nanostructured materials by High pressure Severe Plastic Deformation. *Proceedings of The NATO Advanced study institute*, 2006, 212, 21-28.
65. Raghavendra, N.; Amamurthy, V. S., Effect of particle size and weight fraction of alumina reinforcement on wear behavior of aluminum metal matrix composites, *International Journal of Innovative Research in Science, Engineering and Technology*, 2014, 3 (4), 11191-11198.
66. Stefeneseu, F.; Neagu, G.; Mihai, A., Practical aspect concerning the solidification of cast metallic composites, *UPD science bulletin series B*, 2007, 69, 4.
67. Bodunrina, M. O.; Alanemea, K. K.; Chown, L. H., Aluminum matrix hybrid composites: a review of reinforcement philosophies; mechanical, corrosion and tribological characteristics, *Journal Materials Research and Technology*, 2015, 4 (4), 434-445.

68. Saheb, N.; Khan, M. S.; Hakeem, A. S., Effect of processing on mechanically alloyed and spark plasma sintered Al-Al₂O₃ nanocomposites, *Journal of Nanomaterials*, 2015, 1- 13, article ID 609824.
69. Estrin, Y.; Vinogradov, A., Extreme grain refinement by severe plastic deformation: a wealth of challenging science, *Acta Materialia*, 2013, 61 (3), 782-817.
70. Bhowmik, A.; Biswas, S.; Suwas, S.; Ray, R. K.; Bhattacharjee, D., Evolution of grain-boundary microstructure and texture in interstitial-free steel processed by equal-channel angular extrusion, *Metallurgical and Materials Transactions A*, 2009, 40 (11), 2729-2742.
71. Fogagnolo, J. B.; Robert, M. H.; Navas, E. M .R.; Torralba, J. M., 6061 Al reinforced with zirconium diboride particles processed by conventional powder metallurgy and mechanical alloying, *Journal of Materials Science*, 2004, 39 (1), 127-132.
72. Dunlap, R. A.; Small, D. A.; MacKay, G. R.; O'Brien, J. W.; Dahn, J. R.; Cheng, Z. H., Materials preparation by ball milling. *Canadian Journal of Physics*, 2000, 78, 211-229.
73. Ferrasse, S.; Segal, V. M.; Hartwig, K. T.; Goforth, R. E., Development of a submicrometer grained microstructure in aluminum 6061 using equal channel angular extrusion, *Journal of Materials Research Society*, 1997, 12 (5), 1253-1261.
74. Rao, P. N.; Singh, D.; Jayaganthan, R., Effect of annealing on microstructure and mechanical properties of Al6061 alloy processed by cryorolling, *Materials Science and Technology*, 2013, 29 (1), 76-82.
75. Jimanez, C. M. C.; Gracia, J. M.; Rauch, E. F.; Blandin, J. J.; Ruano, O. A.; Carreno, F., Influence of processing severity during equal-channel angular pressing on the microstructure of an Al-Zn-Mg-Cu alloy. *Metallurgical and Materials Transaction A*, 2012, 43 (11), 4224-4236.
76. Isadare, A. D.; Aremo, B.; Adeoye, M. O.; Olawale, O. J.; Shittu, M. D., Effect of heat treatment on some mechanical properties of 7075 aluminium alloy, *Materials Research*, 2013, 16 (1), 190-194.
77. Kim, J. K.; Jeong, H. G.; Hong, S. I.; Kim, Y. S.; Kim, W. J., Effect on aging treatment on heavily deformed microstructure of AA6061 after ECAP. *Scripta Materialia*, 2001, 45 (8), 901-907.
78. Zhao, Y. H.; Liao, X. z.; Jin, Z.; Valiev, R. Z.; Zhu, Y. T., Microstructures and mechanical properties of ultrafine grained 7075 Al alloy processed by ECAP and their evolutions during annealing, *Acta Materialia*, 2004, 52 (15), 4589-4599.
79. Jimenez, C. M. C.; Infanta, J. M. G.; Ruano, O. A.; Carreno, F., Mechanical properties at room temperature of an Al-Zn-Mg-Cu alloy processed by equal channel angular pressing, *Journal of Alloys and Compounds*, 2011, 509 (35), 8649-8656.

80. Canadinc, D.; Maier, H. J.; Haouaoui, M.; Karaman, I., On the cyclic stability of nanocrystalline copper obtained by powder consolidation at room temperature, *Scripta Materialia*, 2008, 58, 307-310.
81. Zuyan, L.; Zhongjin, W., Finite-element analysis of the load of equal-cross-section lateral extrusion, *Journal of Materials Processing Technology*, 1999, 94, 193–196,
82. Lapovok, R.; Tomus, D.; Muddle, B. C., Low-temperature compaction of Ti–6Al–4V powder using equal channel angular extrusion with back pressure, *Materials Science and Engineering A*, 2008, 490, 171-180.
83. Mani, B.; Jahedi, M.; Paydar, M. H., Consolidation of commercial pure aluminum powder by torsional-equal channel angular pressing (T-ECAP) at room temperature, *Powder Technology*, 2012, 219, 1–8.
84. Valiev, R. Z.; Murashkin, M. Y.; Straumal, B. B., Enhanced ductility in ultrafine-grained Al alloys produced by SPD techniques, *Materials Science Forum*, 2010, 633 (634), 321-332.
85. Jamaati, R.; Toroghinejad, M. R.; Dutkiewicz, J.; Szpunar, J. A., Investigation of nanostructured Al/Al₂O₃ composite produced by ARB process, *Materials and Design*, 2012, 35, 37-42.
86. Azin, A.; Toroghinejad, M. R.; Najafizadeh, A., Evaluation of microstructure and mechanical properties of Al/Al₂O₃/SiC hybrid composite fabricated by accumulative roll bonding process, *Materials and Design*, 2014, 53, 13–19.
87. Shamanian, M.; Mohammadnezhad, M.; Szpunar, J., Fabrication and characterization of Al–Al₂O₃–ZrC composite produced by accumulative roll bonding (ARB) process, *Journal of Alloys and Compounds*, 2015, 618, 19–26.
88. Govindaraj, N. V., Light-weight materials produced by accumulative roll bonding, Norwegian University of Science and Technology *Ph.D Thesis*, 2013, 49-52. .
89. Lihong, S., Microstructure, texture and vacancy-type defect in severe plastic deformation of aluminum alloys, University of Walonggong, *PhD Thesis*, 2012, 165-169.
90. Jamaati, R.; Toroghinejad, M. R., High strength and highly uniform composite produced by anodizing and accumulative roll bonding, *Materials and Design*, 2010, 31 (10), 4816-4822.

LIST OF PUBLICATIONS

1. **Pramono, A.; Kollo, L.; Kallip, K.; Veinthal, R.; Gomon, J. K.**, Heat treatment of ultrafine grained high-strength aluminum alloy. *Key-Engineering Materials*, 2014, 604, 273-276.
2. **Pramono, A.; Kollo, L.; Kallip, K.; Veinthal, R.; Gomon, J. K.**, Heat treatment of ultrafine grained AA6061 consolidation by equal channel angular pressing. *Applied Mechanics and Materials*, 2015, 771, 252-256.
3. **Pramono, A.; Kommel, L.; Kollo, L.; Veinthal, R.**, Hot and cold of pressing effect on equal channel angular pressing (ECAP)-parallel channel composite based Al/ANF material. *Advanced Materials Science and Technology*, 2015, 1123, 343-347.
4. **Pramono, A.; Kollo, R.; Veinthal, R.**, Microstructure of AA7075 based composite by accumulative roll bonding process. *Advanced Materials Science and Technology*, 2015, 1123, 114-118.
5. **Pramono, A.; Kollo, L.; Veinthal, R.**, Hot and cold regions during accumulative roll bonding of Al/Al₂O₃ nanofibre composite. *Proceedings of the Estonian Academy of Sciences*, 2016, 2 (65), 132-137.
6. **Pramono, A.; Kollo, L.; Veinthal, R.**, Aluminum based composite by novelty process: repetitive press roll bonding (RPRB), *Procedia Chemistry*, 2015, 16, 473-479.

Publications not included in the thesis:

7. **Pramono, A.; Kollo, L.; Kallip, K.; Veinthal, R.; Gomon, J. K.**, Processing aluminum by equal channel angular pressing consolidation, *Proceeding of Toward Sustainability and Quality of Life*, 2014, 1, 66-76.
8. **Pramono, A.; Kommel, L.; Kollo, L.; Veinthal, R.**, The aluminum based composite produced by self propagating high temperature synthesis. *Materials Science (Medžiagotyra)*, 2016, 22 (1), 41-44.

ACKNOWLEDGEMENT

First, I would like to thank my supervisor Lauri Kollo, Ph.D, my co-supervisor Lembit Kommel, Ph.D, who have guided and directed with exceptional motivation and provided support for my research work. They have shared their knowledge and research experience sufficient to my career as researcher in the future.

Second, I would like to thank the Ministry Education and Research of Higher Education (DIKTI), Republic Indonesia for full-scholarship, University of Sultan Ageng Tirtayasa for their recommendation of scholarship., PPI Estonia (Indonesian student association in Estonia), and Estonian Ministry of Education and Research.

Third, I appreciate of the whole staff, colleagues and friends in the Department of Materials Engineering, Tallinn University of Technology.

Assoc. Prof. Fjodor Sergejev as Head of Department Materials Engineering and secretary: Sirje Roosme and Mariliis Trei.

Prof. Renno Veinthal, Prof. Priit Kulu, Prof. Jakob Kübarsepp, Prof. Irina Husainova, Dr. Kristjan Juhani, Dr. Juri Pirso, Dr. Priidu Peetsalu, Dr. Maksim Antonov, Dr. Andrei Surženkov, Dr. Dmitri Goljandin and Assoc. Prof Mart Saarna, Hans Vallner, Kaspar Kallip, Der Liang Yung, Mark Kolnes, Marek Taraste, Marek Joeleht, Jaana-Kateriina Gomon, Maria Drozdova, Zorjana Mural, Marina Aghayan, and Diana Matejuk.

Fourth, my thanks are due to Dean of the Faculty of Mechanical Engineering, Tallinn University of Technology; Prof. Tauno Otto, Moonika Asu and Anu Johannes from Research Administration Office.

Many thanks to my friends in the Faculty: Klodian Dhoska, Admire Hoxha, Ahmad Tusef, Kashif Mahmood, Kashif Bajwa, Levon Gevorgov, Vakhtang Mosidze, Maarjus Kirs and so many friends who I cannot mention it one by one.

My special thanks are due to my family for support and affection. Anistasia Milandia Pramono who gave fabulous support and spirit as well. I dedicate all of my science knowledge for civilization and academic community people of Indonesia.

ABSTRACT

Severe Plastic Deformation of Aluminum Based Composites

Metal Matrix Composites are being considered as a group of new advanced materials for their light weight, high strength, low thermal expansion coefficient and good wear resistance. Among metal materials eligible for these properties is aluminum. Aluminum is a non-ferrous metal that has malleability and ductility and good formability. Composite manufacturing technology consists of various processes, such as powder metallurgy, foundry technology and metal forming process. Recent developments of composite materials are the process of Severe Plastic Deformation (SPD), i.e. Equal Channel Angular Pressing (ECAP), High Pressure Torsion (HPT) and Accumulative Roll Bonding (ARB).

The purpose of this study is the use of aluminum as a matrix of composite processed by SPD with different technologies, such as ECAP Consolidation, ECAP Parallel Channel and ARB. The latest method of SPD is RPRB, developed to improve the ARB process to produce highest properties. The process of ARB needs further compression, reaching many cycles, but the RPRB technology already in the third cycle is able to generate interphase bonding between the matrix and reinforcement.

An ECAP consolidation result in ultrafine grain size and following annealing improves the formability of the composite. Quenching and artificial aging after SPD process improves strength properties and higher ductility of the material. During ECAP - PC the importance of temperature on deformation and compaction was studied. For composites with alloy matrix increased temperatures during compaction are crucial for high-density materials. The use of Finite Element analysis supports experimental results in terms of distribution of pressure and temperature during compaction. Also with ARB process the effect of roll diameter in hot and cold regions of deformation was investigated. Comparison of material properties obtained by ARB and newly developed RPRB processes was also performed.

In the results of development of SPD consolidation aluminum alloy 6061 and 7075 powders, ultrafine bulk alloys with acceptable strength and ductility.

ECAP-PC process is viable route to produce Al/Al₂O₃ nanofiber composites.

ARB process enables production of aluminum matrix composites reinforced with aligned nanofibers. Clear evidence of the positive effect of aligned versus non-aligned nanofibers was shown. An important processing parameter was found to be the temperature during compaction – even small deviation below the crystallization temperature induces growth of not desired dendritic structure.

Novel Repetitive Press Roll Bonding technology was proposed, simplifying the ARB process and embedding of Al₂O₃ nanofibers as reinforcement in MMC.

Keywords: Aluminum, Al₂O₃ nanofibers, MMC, SPD, Heat treatment, ECAP, ARB and RPRB.

KOKKUVÕTE

Alumiiniumi baasil komposiitide süvoplastse deformatsiooni protsesside uurimine

Alumiiniumi baasil metallmaatrikskomposiidid (MMK) on kujunenud arvestatavaks kõrgtehnoloogiliste materjalide grupiks tänu nende kergekaalulisusele, suurele tugevusele, väiksele soojuspaisumisele ja heale kulumiskindlusele. MMK tootmisprotsess sisaldab mitmeid protsesse nagu pulbermetallurgia, valutehnoloogia ja survetöötlus.

Käesolevad arengud MMK valdkonnas on seotud süvoplastse deformeerimise (*Severe Plastic Deformation*, SPD), näiteks võrdkanalnurkpressimisega (*Equal Channel Angular Pressing*, ECAP), kõrgsurveväände (*High Pressure Torsion*, HPT) ja summeriva valtsliitmise (*Accumulative Roll Bonding*, ARB) protsessidega.

Käesoleva uurimuse eesmärgiks on alumiiniummaatrikskomposiitide saamine läbi erinevate süvoplastse deformatsiooni protsesside, nagu ECAP ja paralleelkanalitega ECAP (ECAP-PC) ja ARB konsolideerimise. Uusimaks SPD protsessiks on korduvsurvevaltsliitmine (*Repetitive Press Rolling Bonding*, RPRB), parandamaks ARB protsessi tulemusena saadud materjali omadusi. Kui ARB tavaprotsessi korral on vajalik järgnev paljutsükliline survepressimine, siis läbi kolmetsüklilise RPRB protsessi tekitame faasidevahelise sideme maatriksi ja armatuuri vahel. ECAP konsolideerimine tagab meile ülipeene tera, järgnev protsess lõõmutus – hea vormitavuse ning termotöötlus (karastamise ja kunstliku vanandamise) – head tugevus- ja plastsusomadused. Määramaks materjali käitumist ECAP-PC protsessis, uuriti nii külm- kui kuumpressimist. Lõplike elementide meetodi (FEM) kasutamine võimaldas analüüsida pinget ja temperatuuri jaotust deformeerimisel, ARB töötlemisel kuum- ja külmdeformatsiooni alades ka valtside kuju mõju mikrostruktuurile. Võrreldi materjali omadusi, mis saadi ARB ja uusima, RPRB meetodi korral.

Läbi SPD protsesside arenduse on võimalik saada alumiiniumisulamite (6061 ja 7075) pulbrite konsolideerimisega kompaktsid peenterasulameid piisava tugevuse ja sitkusega.

Selgitati välja, et ECAP-PC protsess on sobilik Al/Al₂O₃ nanokiudkomposiitide saamiseks.

ARB protsess võimaldab saada alumiiniummaatriksiga nanokiududega armeeritud komposiite, kusjuures nanokiududega armeerimise efekt oli ilmne. Selgitati, et üheks oluliseks protsessiparameetriks on temperatuur – väike kõrvalekalle kristallisatsioonitemperatuurist tingib deformeerimist raskendavate dendriitide tekke. On pakutud uudne RPRB tehnoloogia, mis lihtsustab ARB protsessi ja Al₂O₃ nanokiudarmatuuri sisseviimist alumiiniummaatriksisse.

ELULOOKIRJELDUS

1. Isikuandmed

Ees- ja perekonnanimi: Agus Pramono
Sünniaeg ja -koht: 18 August 1976, Kediri
Kodakondsus: Indoneesia

2. Kontaktandmed

Address: Akadeemia tee 5-528B, 19086 Tallinn
Telefon: +372 58473788
E-post: agus.pramono@ttu.ee

3. Hariduskäik

Õppeasutus (nimetus lõpetamise ajal)	Lõpetamise aeg	Haridus (eriala/kraad)
Indoneesia Ülikool	2005 - 2007	Magistriõpe, Metallurgia
Merdeka Ülikool	1995 - 2000	Bakalaureuseõpe, Mehaanika

4. Keelteoskus (alg-, kesk- või kõrgtase)

Keel	Tase
Indoneesia keel	kõrgtase
Jaava keel	emakeel
Inglise keel	kõrgtase
Araabia keel	kesktase
Eesti keel	algtase
Vene keel	algtase

5. Teenistuskäik

Periood	Organisatsioon	Asukoht
2014 - 2016	Indonesian Students Association in Estonia	Juhatuse liige
2010 - täna	Indonesian Welding Society	Instruktor
2010 - 2012	Composites Association of Indonesia	Juhatuse liige

6. Professionaalsed tööhõived

Periood	Tööhõive	Asukoht
2008 - täna	University of Sultan Ageng, Tirtayasa Indonesia	Vanem õppejõud
2001 - 2005	University Merdeka of Malang, Indonesia	Noorem õppejõud

CURRICULUM VITAE

1. Personal data

Name : Agus Pramono
Date and place of birth : 18 August 1976 / Kediri, Indonesia

2. Contact information

Address : Akadeemia tee 5-528B, 19086 Tallinn
Phone : +372 58473788
E-mail : agus.pramono@ttu.ee

3. Education

Educational institution	Graduation year	Education (field of study/degree)
University of Indonesia	2005 - 2007	Master of Engineering, (M.Eng.)
University Merdeka of Malang	1995 - 2000	Mechanical Engineering (Bachelor of Eng.)
Kediri State High School 1	1993 - 1995	(High School Education)

4. Language competence/skills (fluent, average, basic skills)

Language	Level
Indonesian	fluent
Javanese	fluent (mother tongue)
English	good
Arabic	intermediate
Estonian	basic skills
Russian	basic skills

5. Professional Organization

Period	Organization	Position
2014 - 2016	Indonesian Students Association in Estonia	Chairman
2010 - present	Indonesian Welding Society	Instructor
2010 - 2012	Composites Association of Indonesia	Chairman

6. Professional Employment

Period	Institution	Position
2008 - present	University of Sultan Ageng, Tirtayasa Indonesia	Senior Lecturer
2001 - 2005	University Merdeka of Malang, Indonesia	Early Stage Lecturer

**DISSERTATIONS DEFENDED AT
TALLINN UNIVERSITY OF TECHNOLOGY ON
*MECHANICAL ENGINEERING***

1. **Jakob Kübarsepp**. Steel-Bonded Hardmetals. 1992.
2. **Jakub Kõo**. Determination of Residual Stresses in Coatings & Coated Parts. 1994.
3. **Mart Tamre**. Tribocharacteristics of Journal Bearings Unlocated Axis. 1995.
4. **Paul Kallas**. Abrasive Erosion of Powder Materials. 1996.
5. **Jüri Pirso**. Titanium and Chromium Carbide Based Cermets. 1996.
6. **Heinrich Reshetnyak**. Hard Metals Serviceability in Sheet Metal Forming Operations. 1996.
7. **Arvi Kruusing**. Magnetic Microdevices and Their Fabrication methods. 1997.
8. **Roberto Carmona Davila**. Some Contributions to the Quality Control in Motor Car Industry. 1999.
9. **Harri Annuka**. Characterization and Application of TiC-Based Iron Alloys Bonded Cermets. 1999.
10. **Irina Hussainova**. Investigation of Particle-Wall Collision and Erosion Prediction. 1999.
11. **Edi Kulderknup**. Reliability and Uncertainty of Quality Measurement. 2000.
12. **Vitali Podgurski**. Laser Ablation and Thermal Evaporation of Thin Films and Structures. 2001.
13. **Igor Penkov**. Strength Investigation of Threaded Joints Under Static and Dynamic Loading. 2001.
14. **Martin Eerme**. Structural Modelling of Engineering Products and Realisation of Computer-Based Environment for Product Development. 2001.
15. **Toivo Tähemaa**. Assurance of Synergy and Competitive Dependability at Non-Safety-Critical Mechatronics Systems design. 2002.
16. **Jüri Resev**. Virtual Differential as Torque Distribution Control Unit in Automotive Propulsion Systems. 2002.
17. **Toomas Pihl**. Powder Coatings for Abrasive Wear. 2002.
18. **Sergei Letunovitš**. Tribology of Fine-Grained Cermets. 2003.
19. **Tatyana Karaulova**. Development of the Modelling Tool for the Analysis of the Production Process and its Entities for the SME. 2004.
20. **Grigori Nekrassov**. Development of an Intelligent Integrated Environment for Computer. 2004.
21. **Sergei Zimakov**. Novel Wear Resistant WC-Based Thermal Sprayed Coatings. 2004.

22. **Irina Preis.** Fatigue Performance and Mechanical Reliability of Cemented Carbides. 2004.
23. **Medhat Hussainov.** Effect of Solid Particles on Turbulence of Gas in Two-Phase Flows. 2005.
24. **Frid Kaljas.** Synergy-Based Approach to Design of the Interdisciplinary Systems. 2005.
25. **Dmitri Neshumayev.** Experimental and Numerical Investigation of Combined Heat Transfer Enhancement Technique in Gas-Heated Channels. 2005.
26. **Renno Veinthal.** Characterization and Modelling of Erosion Wear of Powder Composite Materials and Coatings. 2005.
27. **Sergei Tisler.** Deposition of Solid Particles from Aerosol Flow in Laminar Flat-Plate Boundary Layer. 2006.
28. **Tauno Otto.** Models for Monitoring of Technological Processes and Production Systems. 2006.
29. **Maksim Antonov.** Assessment of Cermets Performance in Aggressive Media. 2006.
30. **Tatjana Barashkova.** Research of the Effect of Correlation at the Measurement of Alternating Voltage. 2006.
31. **Jaan Kers.** Recycling of Composite Plastics. 2006.
32. **Raivo Sell.** Model Based Mechatronic Systems Modeling Methodology in Conceptual Design Stage. 2007.
33. **Hans Rämmal.** Experimental Methods for Sound Propagation Studies in Automotive Duct Systems. 2007.
34. **Meelis Pohlak.** Rapid Prototyping of Sheet Metal Components with Incremental Sheet Forming Technology. 2007.
35. **Priidu Peetsalu.** Microstructural Aspects of Thermal Sprayed WC-Co Coatings and Ni-Cr Coated Steels. 2007.
36. **Lauri Kollo.** Sinter/HIP Technology of TiC-Based Cermets. 2007.
37. **Andrei Dedov.** Assessment of Metal Condition and Remaining Life of In-service Power Plant Components Operating at High Temperature. 2007.
38. **Fjodor Sergejev.** Investigation of the Fatigue Mechanics Aspects of PM Hardmetals and Cermets. 2007.
39. **Eduard Ševtšenko.** Intelligent Decision Support System for the Network of Collaborative SME-s. 2007.
40. **Rünno Lumiste.** Networks and Innovation in Machinery and Electronics Industry and Enterprises (Estonian Case Studies). 2008.
41. **Kristo Karjust.** Integrated Product Development and Production Technology of Large Composite Plastic Products. 2008.

42. **Mart Saarna**. Fatigue Characteristics of PM Steels. 2008.
43. **Eduard Kimmari**. Exothermically Synthesized B₄C-Al Composites for Dry Sliding. 2008.
44. **Indrek Abiline**. Calibration Methods of Coating Thickness Gauges. 2008.
45. **Tiit Hindreus**. Synergy-Based Approach to Quality Assurance. 2009.
46. **Karl Raba**. Uncertainty Focused Product Improvement Models. 2009.
47. **Riho Tarbe**. Abrasive Impact Wear: Tester, Wear and Grindability Studies. 2009.
48. **Kristjan Juhani**. Reactive Sintered Chromium and Titanium Carbide-Based Cermets. 2009.
49. **Nadežda Dementjeva**. Energy Planning Model Analysis and Their Adaptability for Estonian Energy Sector. 2009.
50. **Igor Krupenski**. Numerical Simulation of Two-Phase Turbulent Flows in Ash Circulating Fluidized Bed. 2010.
51. **Aleksandr Hlebnikov**. The Analysis of Efficiency and Optimization of District Heating Networks in Estonia. 2010.
52. **Andres Petritšenko**. Vibration of Ladder Frames. 2010.
53. **Renee Joost**. Novel Methods for Hardmetal Production and Recycling. 2010.
54. **Andre Gregor**. Hard PVD Coatings for Tooling. 2010.
55. **Tõnu Roosaar**. Wear Performance of WC- and TiC-Based Ceramic-Metallic Composites. 2010.
56. **Alina Sivitski**. Sliding Wear of PVD Hard Coatings: Fatigue and Measurement Aspects. 2010.
57. **Sergei Kramanenko**. Fractal Approach for Multiple Project Management in Manufacturing Enterprises. 2010.
58. **Eduard Latõsov**. Model for the Analysis of Combined Heat and Power Production. 2011.
59. **Jürgen Riim**. Calibration Methods of Coating Thickness Standards. 2011.
60. **Andrei Surzhenkov**. Duplex Treatment of Steel Surface. 2011.
61. **Steffen Dahms**. Diffusion Welding of Different Materials. 2011.
62. **Birthe Matsi**. Research of Innovation Capacity Monitoring Methodology for Engineering Industry. 2011.
63. **Peeter Ross**. Data Sharing and Shared Workflow in Medical Imaging. 2011.
64. **Siim Link**. Reactivity of Woody and Herbaceous Biomass Chars. 2011.
65. **Kristjan Plamus**. The Impact of Oil Shale Calorific Value on CFB Boiler Thermal Efficiency and Environment. 2012.
66. **Aleksei Tšinjan**. Performance of Tool Materials in Blanking. 2012.

67. **Martinš Sarkans**. Synergy Deployment at Early Evaluation of Modularity of the Multi-Agent Production Systems. 2012.
68. **Sven Seiler**. Laboratory as a Service – A Holistic Framework for Remote and Virtual Labs. 2012.
69. **Tarmo Velsker**. Design Optimization of Steel and Glass Structures. 2012.
70. **Madis Tiik**. Access Rights and Organizational Management in Implementation of Estonian Electronic Health Record System. 2012.
71. **Marina Kostina**. Reliability Management of Manufacturing Processes in Machinery Enterprises. 2012.
72. **Robert Hudjakov**. Long-Range Navigation for Unmanned Off-Road Ground Vehicle. 2012.
73. **Arkadi Zikin**. Advanced Multiphase Tribo-Functional PTA Hardfacings. 2013.
74. **Alar Konist**. Environmental Aspects of Oil Shale Power Production. 2013.
75. **Inge Roos**. Methodology for Calculating CO₂ Emissions from Estonian Shale Oil Industry. 2013.
76. **Dmitri Shvarts**. Global 3D Map Merging Methods for Robot Navigation. 2013.
77. **Kaia Lõun**. Company's Strategy Based Formation of e-Workplace Performance in the Engineering Industry. 2013.
78. **Maido Hiiemaa**. Motion Planner for Skid-Steer Unmanned Ground Vehicle. 2013.
79. **Dmitri Goljandin**. Disintegrator Milling System Development and Milling Technologies of Different Materials. 2013.
80. **Dmitri Aleksandrov**. Light-Weight Multicopter Structural Design for Energy Saving. 2013.
81. **Henrik Herranen**. Design Optimization of Smart Composite Structures with Embedded Devices. 2014.
82. **Heiki Tiikoja**. Experimental Acoustic Characterization of Automotive Inlet and Exhaust System. 2014.
83. **Jelena Priss**. High Temperature Corrosion and Abrasive Wear of Boiler Steels. 2014.
84. **Aare Aruniit**. Thermoreactive Polymer Composite with High Particulate Filler Content. 2014.
85. **Dmitri Gornostajev**. Development of the Calculation Method for Barge Hull. 2014.
86. **Liina Lind**. Wear of PVD Coatings on Fineblanking Punches. 2014.
87. **Nikolai Voltšihhin**. Design and Technology of Oxides-Containing Ceramic-Based Composites. 2014.

88. **Aleksander Šablinski.** RANS Numerical Modelling of Turbulent Polydispersed Flows in CFB Freeboard. 2015.
89. **Tanel Aruväli.** Wireless Real-time Monitoring of Machining Processes. 2015.
90. **Andrei Bogatov.** Morphological Changes on Diamond and DLC Films During Sliding Wear. 2015.
91. **Raimo Kabral.** Aero-Acoustic Studies and Innovative Noise Control with Application to Modern Automotive Gas Exchange System. 2015.
92. **Jevgeni Sahno.** Dynamic Management Framework for Continuous Improvement of Production Processes. 2015.
93. **Ott Pabut.** Optimal Design of Slotless Permanent Magnet Generators. 2015.
94. **Merili Kukuškin.** Value Centric Business Development for Estonian Manufacturing Small and Medium Sized Enterprises. 2015.
95. **Kaimo Sonk.** Development of Additive Manufacturing Based on Functional Requirements. 2015.
96. **Marina Aghayan.** Functionalization of Alumina Nanofibers with Metal Oxides. 2016.
97. **Marek Jõelett.** Titanium Carbide Cermet as Ballistic Protection Material. 2016.
98. **Heikki Sarjas.** Novel Synthesized and Milled Carbide-based Composite Powders for HVOF Spray. 2016.
99. **Klodian Dhoska.** Measurement Methods with 3D Coordinate Measuring Machine and Improved Characterization Setup for Detector Performance. 2016.
100. **Aleksei Snatkin.** Development and Optimisation of Production Monitoring System. 2016.
101. **Igor Poljantšikov.** Partners Selection Tool for Virtual Enterprise in SMEs Network. 2016.
102. **Sergei Žigailov.** Experimental and Analytical Modelling of Pelvic Motion. 2016.
103. **Rommi Källo.** Synergy-Based Chaos Control in the Multi-Agent Hierarchical Systems. 2016.
104. **Der-Liang Yung.** ZrC-based and ZrC-doped Composites for High-Temperature and Wear Applications. 2016.
105. **Viive Pille.** Development of a Model for the Prevention of Work-Related Musculoskeletal Disorders in the Upper Extremities. 2016.